Title
Ty3 capsid mutations reveal early and late functions of the amino-terminal domain.

Journal
Journal of virology, 81(13)

ISSN
0022-538X

Authors
Larsen, Liza SZ
Zhang, Min
Beliakova-Bethell, Nadejda
et al.

Publication Date
2007-07-01

DOI
10.1128/jvi.02207-06

JOURNAL OF VIROLOGY, July 2007, p. 6957–6972 Vol. 81, No. 13
0022-538X/07/$08.00+0 doi:10.1128/JVI.02207-06

Ty3 Capsid Mutations Reveal Early and Late Functions of the Amino-Terminal Domain▽

Liza S. Z. Larsen,[1,3]† Min Zhang,[2]† Nadejda Beliakova-Bethell,[2] Virginia Bilanchone,[2] Anne Lamsa,[2] Kunio Nagashima,[4] Rani Najdi,[1] Kathryn Kosaka,[1] Vuk Kovacevic,[2] Jianlin Cheng,[3]‡ Pierre Baldi,[3] G. Wesley Hatfield,[1,3] and Suzanne Sandmeyer[1,2,3]*

Departments of Microbiology and Molecular Genetics[1] and Biological Chemistry[2] and School of Information and Computer Sciences and Institute for Genomics and Bioinformatics,[3] University of California, Irvine, California 92697, Image Analysis Laboratory, NCI-Frederick, SAIC-Frederick, Inc., Frederick, Maryland 21702[4]

Received 8 October 2006/Accepted 26 March 2007

The Ty3 retrotransposon assembles into 50-nm virus-like particles that occur in large intracellular clusters in the case of wild-type (wt) Ty3. Within these particles, maturation of the Gag3 and Gag3-Pol3 polyproteins by Ty3 protease produces the structural proteins capsid (CA), spacer, and nucleocapsid. Secondary and tertiary structure predictions showed that, like retroviral CA, Ty3 CA contains a large amount of helical structure arranged in amino-terminal and carboxyl-terminal bundles. Twenty-six mutants in which alanines were substituted for native residues were used to study CA subdomain functions. Transposition was measured, and particle morphogenesis and localization were characterized by analysis of protein processing, cDNA production, genomic RNA protection, and sedimentation and by fluorescence and electron microscopy. These measures defined five groups of mutants. Proteins from each group could be sedimented in a large complex. Mutations in the amino-terminal domain reduced the formation of fluorescent Ty3 protein foci. In at least one major homology region mutant, Ty3 protein concentrated in foci but no wt clusters of particles were observed. One mutation in the carboxyl-terminal domain shifted assembly from spherical particles to long filaments. Two mutants formed foci separate from P bodies, the proposed sites of assembly, and formed defective particles. P-body association was therefore found to be not necessary for assembly but correlated with the production of functional particles. One mutation in the amino terminus blocked transposition after cDNA synthesis. Our data suggest that Ty3 proteins are concentrated first, assembly associated with P bodies occurs, and particle morphogenesis concludes with a post-reverse transcription, CA-dependent step. Particle formation was generally resistant to localized substitutions, possibly indicating that multiple domains are involved.

Retrotransposons occur widely in eukaryotic species. Some classes, such as the Ty3/gypsy-like elements (*Metaviridae*), are similar to retroviruses in organization and even in specific sequence features of structural proteins (30). However, these mobile elements typically do not encode matrix or envelope functions, and they assemble and disassemble within a single host cell. Compared to retroviruses, relatively little is known about where they assemble and what protein domains are involved in this process. The present study was undertaken to examine the role of Ty3 capsid (CA) subdomains in localization, assembly, reverse transcription, and transposition.

Although many questions remain concerning the roles of specific retrovirus CA subdomains, knowledge of retrovirus particle structure (21) can inform the design of experiments to define the process of retrotransposon assembly. The major retrovirus structural polyprotein is encoded by the first, or *gag*, open reading frame (ORF). Although the Gag sequence is not highly conserved, its derivative matrix (MA), CA, and nucleocapsid (NC) proteins in different viruses share motifs related to common functions. The *pol* reading frame is typically expressed as part of a Gag-Pol fusion protein that includes domains for protease (PR), reverse transcriptase (RT), and integrase (IN).

In the immature, spherical retrovirus particle, Gag molecules are aligned side by side and extend radially from the NC domain in the particle interior to the MA domain on the exterior (33, 102). MA proteins of retroviruses are implicated in localization of assembly to membranes or to the microtubule organizing complex (74, 82, 85, 103). Particle formation is dependent on the carboxyl-terminal domain (CTD) of CA and spacer and the I domain of NC, with contributions from different domains dominating in different viruses (1, 23, 32, 73, 95, 96, 99; reviewed in references 3, 64, 82, 98, and 100). During assembly, PR is activated upon dimerization (14) and, coordinately with budding, polyprotein precursors are processed into mature forms.

After proteolysis, the enveloped virion reorganizes into its characteristic spherical, conical, or cylindrical mature form, the outer shell of which is composed of CA. Studies of the human T-cell lymphotrophic virus type 1 (HTLV-1), Rous sarcoma virus (RSV), human immunodeficiency virus type 1 (HIV-1), and equine infectious anemia virus (EIAV) CA proteins report a common structure, including an amino-terminal domain (NTD) consisting of a β hairpin followed by a bundle of α helices linked through an unstructured region to a CTD of a smaller α-helical bundle terminating in an unstructured region

* Corresponding author. Mailing address: Department of Biological Chemistry, University of California, Irvine, CA 92697. Phone: (949) 824-7571. Fax: (949) 824-2688. E-mail: sbsandme@uci.edu.
† Liza S. Z. Larsen and Min Zhang contributed equally to this work.
‡ Present address: School of Electrical Engineering and Computer Science, University of Central Florida, Orlando, FL 32816-2362.
▽ Published ahead of print on 18 April 2007.

(8, 10, 17, 20, 34, 35, 39, 48, 50, 51, 62, 63). Electron microscopic (EM) images of assemblies of Gag and CA in lipid monolayers and virus core particles indicate that these molecules assemble into hexameric lattices (4, 5, 12, 36, 58, 67, 102). A recent X-ray crystal analysis shows that the N-tropic murine leukemia virus (MLV) CA NTD forms a hexamer with the amino-terminal three helices mediating intermolecular interactions (65). Consistent with that key position in the structure, Ala-scanning mutagenesis of HIV-1 CA supports a role for the NTD in the transition from immature to mature particle morphology (37, 93, 94) and particle stability (31). The major homology region (MHR), a 19-amino-acid (aa) motif, begins at the distal end of the linker region between the NTD and CTD α-helical regions and overlaps the first helix of the CTD. Mutations within the MHR have pleiotropic effects, including disruption of particle formation and cDNA synthesis, but its precise molecular function remains unknown (100).

Ty3 is 5.4 kb in length and is comprised of 340-bp long terminal repeats (LTRs) flanking *GAG3* and *POL3* ORFs (reviewed in reference 81) (Fig. 1A). *GAG3* encodes CA, spacer, and NC domains (41, 54, 55, 70) (Fig. 1B). *POL3* encodes PR, RT, and IN domains. Gag3 is translated from the first ORF, and, as in many retroviruses, Gag3-Pol3 is produced via a programmed frameshift. The 290-aa Gag3 polyprotein is processed by Ty3 PR (53) into a 206-aa CA (lacking the initiation Met) and a 57-aa NC (53, 55). A 26-aa spacer is inferred to be generated from these cleavages but has not yet been observed. The CA domain contains a copy of the MHR motif, and mutations in this motif have pleiotropic effects (69). Ty3 CA has a copy of the late motif YPXL (26, 64), but its function is not known. Ty3 NC contains one zinc binding domain, which is required for virus-like particle (VLP) formation (70). Cells in which Ty3 is expressed accumulate VLPs that are roughly 50 nm in diameter and have features of icosahedral symmetry (55). It is presumed that, similar to what occurs in retrovirus maturation, incorporation of Gag3-Pol3 into particles is required for proteolytic maturation. Processing bodies (P bodies) are sites of nontranslating RNAs associated with decapping, degradation, and RNA storage in yeast (11, 86). Ty3 transposition frequency and localization are affected by deletion of the *DHH1* and *XRN1* genes, which encode RNA P-body components, and Ty3 CA and RNA colocalize with P-body components. P bodies are therefore proposed to be sites of VLP assembly (6).

Ty3 is the sole representative of the *Metaviridae* in *Saccharomyces cerevisiae.* Other *S. cerevisiae* retrotransposons (Ty1, Ty2, Ty4, and Ty5) are members of the copia-like class (*Pseudoviridae*). The Ty3 VLP has an external structure similar to what has been observed for the Ty1 VLP (55, 77). However, Ty3 is more similar to retroviruses than to Ty1 in organization and sequence of coding domains (30).

The present study was undertaken to define the functional subdomains of Ty3 CA by using 26 Ala substitution mutants. Mutants were characterized for VLP formation, RNA packaging, cDNA production, transposition, and Ty3 protein and particle localization. All but a few of the mutants were able to form particles. However, most were affected in some aspect of particle function. Mutant phenotypes implicated Ty3 CA in processes including localization of Gag3, packaging of genomic

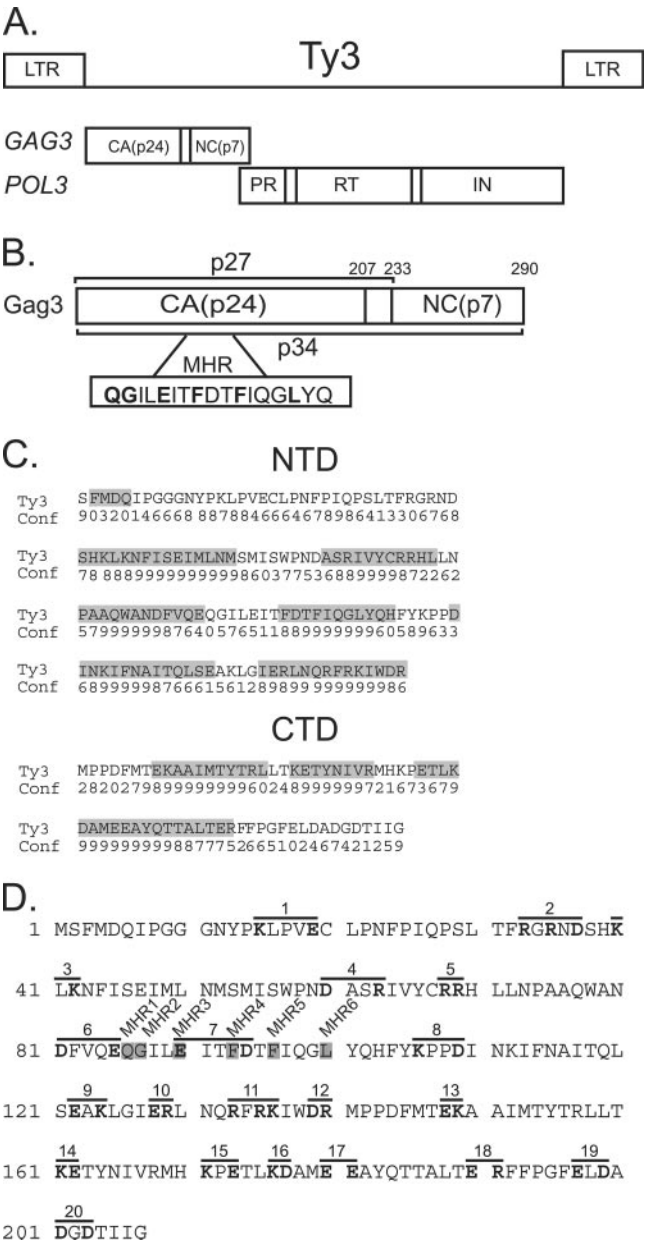

FIG. 1. Ty3 Gag3. (A) Ty3 genome and polyprotein organization. (B) Ty3 Gag3 processing. PR processing of Gag3 results in p34 (aa 1 to 290), p27 (aa 1 to 233), and CA p24 (aa 1 to 207). The conserved MHR domain is indicated in the lower box. The final Phe is a weakly conserved hydrophobic/Ala residue in retrovirus MHR sequences. Ty3 MHR sequences are shown (aa 86 to 104). (C) Predicted helical domains of Ty3 CA. Consensus predictions of Ty3 CA NTD and CTD helical regions were made with SSpro4, PSIPRED, ProfSec, SAM-T99, and SABLE2. The numbers on the "Conf" line are the confidence scores of secondary structure predictions given by PSIPRED. The magnitude of the number correlates with confidence. The helical regions are shaded gray; all nonshaded regions are loops. (D) Ala-scanning mutagenesis of Ty3 CA. Ala-scanning windows containing two or more charged residues are overlined. Mutations 1 to 20 are shown with the substituted positions in bold type, and the six single replacement MHR mutations are shown boxed in gray.

TABLE 1. Primers used to create CA mutations

Primer	Ty3 CA mutation(s)	5′–3′ (forward) sequence[a]
1	K15A/E19A	GGAGGAAATTATCCAGCACTCCCAGTAGCATGCCTTCCTAAC
2	R33A/R35A/D37A	CCAACCATCTTTGACCTTCGCAGGTGCAAATGCCTCGCATAAAC
3	K40A/K42A	CAGAGGTAGAAATGACTCGCATGCACTGGCAAACTTTATCTCCG
4	D60A/R63A	GATATCTTGGCCGAATGCTGCCAGTGCTATTGTGTACTGCAG
5	R68A/R69A	CAGTCGTATTGTGTACTGCGCAGCACATTTATTAAACCCCGCTGC
6	D81A/E85A	GCTCAGTGGGCTAATGCCTTTGTACAAGCACAAGGTATAC
7	E90A/D94A	GAACAAGGTATACTTGCAATAACATTCGCCACATTCATACAAGG
8	K106A/D109A	GGATTATATCAGCATTTCTATGCCCCACCAGCTATCAATAAAATC
9	E122A/K124A	GCAATCACGCAACTTTCCGCAGCTGCACTTGGTATTGAGCGTCTC
10	E128A/R129A	CCGAAGCTAAACTTGGTATTGCCGCTCTCAACCAACGATTCAG
11	R133A/R135A/K136A	GCGTCTCAACCAAGCATTCGCAGCCATTTGGGACAGAATGCCACC
12	D139A/R140A	GATTCAGAAAGATTTGGGCCGCAATGCCACCAGACTTCATGACCG
13	E148A/K149A	GCCACCAGACTTCATGACCGCAGCAGCTGCCATAATGAC
14	K161A/E162A	CTAGGCTATTGACAGCCGCAACCTATAATATTGTCAGAATGCAC
15	K171A/E173A	GTCAGAATGCACGCACCAGCCACATTAAAAGACGCCATGGAAGAG
16	K176A/D177A	GCACAAACCAGAGACATTAGCAGCCGCCATGGAAGAGGCTTACC
17	E180A/E181A	GAGACATTAAAAGACGCCATGGCAGCCGCTTACCAGACAACTGC
18	E190A/R191A	CCAGACAACTGCACTAACTGCAGCATTCTTCCCAGGATTCG
19	E197A/D199A	CCCAGGATTCGCACTTGCTGCTGATGGAGACACTATCATCGG
20	D201A/D203A	CGAACTTGATGCTGCTGGAGCCACTATCATCGGTGCCAC
21	Q86A (MHR1)	GCTCAGTGGGCTAATGACTTTGTACAAGAAGCAGGTATACTTG
22	G87A (MHR2)	GACTTTGTACAAGAACAAGCTATACTTGAAATAACATTCGACAC
23	E90A (MHR3)	GTACAAGAACAAGGTATACTTGCAATAACATTCGACACATTC
24	F93A (MHR4)	GAACAAGGTATACTTGAAATAACAGCCGACACATTCATACAAGG
25	F96A (MHR5)	CATTCGACACAGCCATACAAGGATTATATCAGCATTTCTATAAGC
26	L100A (MHR6)	CGACACATTCATACAAGGAGCATATCAGCATTTCTATAAGCCACC

[a] Mutated codons are underlined.

RNA, proteolytic maturation, and even retrotransposition of cDNA.

MATERIALS AND METHODS

Strains and culture conditions for *S. cerevisiae* and *Escherichia coli*. Yeast strain yTM443 (*MAT***a** *ura3-52 trp1-H3 his3-Δ200 ade2-101 lys2-1 leu1-12 can1-100 bar1*::*hisG* Ty3 null) (61) was used unless otherwise specified. For EM and fluorescence microscopy, yeast strain BY4741 was used (*MAT***a** *his3-Δ1 leu2Δ0 met15Δ0 ura3Δ0*) (Open Biosystems, Huntsville, AL). Yeast transformations were performed by the lithium acetate procedure (84). Rich medium for *S. cerevisiae* cultures was YPD (1% yeast extract–2% peptone–2% dextrose). In order to select for cells with particular prototrophic markers, synthetic dextrose (SD) medium (0.67% yeast nitrogen base–2% dextrose), synthetic galactose (SG) medium (0.67% yeast nitrogen base–2% galactose), or raffinose medium (0.67% yeast nitrogen base–1% raffinose–2% [vol/vol] glycerol–2% [vol/vol] lactic acid) containing complete amino acids minus the appropriate amino acid was used. Yeast growth was as described previously (85a). *E. coli* strain DH5α [F^- ϕ80*lacZ*Δ*M15* Δ(*lacZYA-argF*)*U169 deoR recA1 endA1 hsdR17*(r_K^- m_K^+) *phoA supE44 thi-1 gyrA96 relA1* λ^-] (Invitrogen, Carlsbad, CA) was used for DNA cloning and plasmid preparation.

Plasmid constructions and mutagenesis. All complementary primers containing site-directed mutations (Table 1) were purchased from Integrated DNA Technology (Coralville, IA). All mutants were created in the pGEM3Zf(+)-GAG3 plasmid, which was constructed by ligation of the 2,235-bp BamHI-KpnI Ty3 fragment of plasmid pDLC201 (formerly pEGTy3-1, 2μ, *URA3*, galactose-inducible Ty3-1) (42) into the BamHI-KpnI sites of pGEM3Zf(+) (Promega, Madison, WI). The pGEM3Zf(+)-GAG3 plasmid was isolated from DH5α cells and used as a template for QuikChange mutagenesis, according to the manufacturer's instructions (Stratagene Inc., Cesar Creek, TX). The sequences of mutated plasmids were determined (Cogenics Inc., Houston, TX). pGEM3Zf(+)-GAG3 mutants with sequence-verified mutations were selected and digested with BamHI and KpnI and ligated into the BamHI-KpnI sites of pDLC201. Each mutation was verified after recloning into pDLC201.

In order to localize mutant Ty3 relative to P bodies, the putative assembly site, Ty3 marked with red fluorescent protein (RFP) was expressed in a strain in which a P-body marker protein was fused to green fluorescent protein (GFP). This strategy was previously described and used to show that wild-type (wt) Ty3 proteins are concentrated in P bodies. In the Ty3-RFP construct previously described (6), the coding region for RFP optimized for expression in *S. cerevisiae* (Coda Genomics, Inc., Laguna Hills, CA) was fused in frame to the end of the Ty3 *POL3* reading frame in the high-copy-number expression vector pDLC201. Ty3-RFP expression and VLP formation result in PR processing of Gag3-Pol3 and generation of an IN-RFP fusion. Twenty-one Ty3-RFP CA mutant variants were created by substituting the BamHI-KpnI fragment containing the mutation in the respective pDLC201-based plasmid for the wt version of this fragment in Ty3-RFP. The presence of the mutation in the full-length Ty3 was reconfirmed by DNA sequence analysis of the region containing the mutation (Cogenics Inc.).

Structure predictions. The secondary structure of the Ty3 CA protein was predicted by a consensus approach. The secondary structures of Ty3 CA are consensus predictions made by SSpro4 (19), PSIPRED (13), ProfSec (76), SAM-T99 (49), and SABLE2 (2). As the accuracy of these state-of-the-art secondary structure predictors is high (about 75 to 80%), but not perfect, the confidence scores of the secondary structure predictions generated by PSIPRED were included. The confidence scores for each position range from 0 to 9 (low confidence to high). The secondary structure prediction showed that, like retrovirus CA proteins, Ty3 CA is high in helical structure.

The tertiary structure of Ty3 CA was also predicted, based on the assumption that it shares its structural fold with retrovirus CA proteins. To test the validity of this assumption, the Ty3 CA was submitted to several recognition (or threading) servers to look for similar structures. Surprisingly, one server, FFAS03 (47), ranked HTLV-1 (50), HIV-1 (8, 20, 63), RSV (17), and EIAV (10) CA proteins within the top 10 templates, despite the lack of sequence similarity between Ty3 CA and the other CA proteins. More specifically, the CA proteins of EIAV and HIV-1 ranked first and second, respectively. Two other recognition servers, Meta-BASIC (38) and FOLDpro (18), also ranked one of the retrovirus proteins within the top templates. Although not all recognition servers returned one or more retrovirus CA proteins as templates, the overlap between the independent predictions made by FFAS03, MetaBASIC, and FOLDpro provides some evidence that Ty3 CA may have a nontrivial degree of structural similarity with other retrovirus CA proteins.

To further assess the tertiary structure of Ty3 CA, the sequences and structures of the CA proteins of HTLV-1 (1QRJ) (50), RSV (1D1D) (17, 51), EIAV (1IEA) (10), and HIV-1 (1E6J) (8, 39, 63) were extracted from the Protein Data Bank (7). Because sequence similarity between the Ty3 CA protein and other retroviruses is very low, profile-profile alignment methods, which are more sensitive than sequence-sequence or profile-sequence alignment methods, were used to align the Ty3 CA protein with the four retrovirus proteins. The profiles of Ty3

CA and the other four proteins were generated by using PSI-BLAST to search the nonredundant protein sequence database. The profile of the Ty3 CA protein was aligned with those of the four retroviruses by ClustalW (90) and PALIGN (68). ClustalW and PALIGN generated almost exactly the same alignments for Ty3 and HIV-1 and very similar alignments for Ty3 and EIAV, but the alignments with HTLV-1 and RSV were more divergent. Thus, we chose to use the HIV-1 CA template to predict the structure of Ty3 CA. Based on the alignment of HIV-1 CA and Ty3 CA generated by ClustalW, Modeler (79) was used to generate the energy minimized tertiary structure of Ty3 CA.

Transposition assays. Transposition was measured with a target plasmid assay described previously (52). Transposition was induced from Ty3 under transcriptional control of the *GAL1-10* upstream activation sequence (UAS) on a plasmid by growth on galactose-containing medium. Transposition of Ty3 into the low-copy-number target plasmid pCH2bo19V activates expression of a suppressor tRNA gene. Transposition is scored by growth dependent on suppression of the ochre nonsense alleles *ade2-101* and *lys2-1* in yeast strain yTM443 (52, 61). Transposition assays were performed at 24°C and 30°C. Under these conditions, four independent transformants for each mutant were patched onto SD-Ura-His medium. After 1 day, cells were replica plated to SG-Ura-His to induce transposition. After 2 days, cells were replica plated to minimal medium supplemented with Leu and Trp to select for Ade^+ and Lys^+ colonies.

Immunoblot analysis of Ty3 intermediates in extracts of cells expressing Ty3. Two transformants containing pDLC201 wt or mutant derivative plasmid and target plasmid were grown overnight at 30°C in 3 ml of noninducing synthetic raffinose (SR)-Ura medium. Five milliliters of SR-Ura was added to the 3-ml overnight culture. Cells were grown for 5 h, diluted into inducing medium (2% SG-Ura) to a final optical density at 600 nm (OD_{600}) of 0.35, and grown for 24 h at 24°C. Whole-cell extracts (WCEs) were prepared from 5-ml cultures by vortexing with glass beads in the presence of denaturing buffer (9 M urea–5 mM EDTA) (Continental Labs, Carlsbad, CA), as previously described. WCEs were fractionated by electrophoresis in a 4 to 20% sodium dodecyl sulfate (SDS)-polyacrylamide gel (Pierce Biotechnology, Inc., Rockford, IL). Proteins were transferred to Immobilon-P membranes (Millipore, Bedford, MA) and were incubated with rabbit polyclonal anti-Ty3 CA or anti-Ty3 IN antibodies diluted 1:20,000 and 1:2,000, respectively (61). Rabbit immunoglobulin G was visualized with horseradish peroxidase-conjugated secondary antibody and ECL Plus (Amersham, Buckinghamshire, United Kingdom), according to the manufacturer's instructions. The blot used to probe for IN was also used to probe for phosphoglycerate kinase (PGK) by using anti-phosphoglycerate kinase immunoglobulin G (Invitrogen, Carlsbad, CA) (data not shown).

Southern blot analysis of Ty3 cDNA in extracts of cells expressing Ty3. Cells of yeast strain yTM443 transformed with pDLC201 mutant derivative plasmids and the target plasmid pCH2bo19V were grown as described above for immunoblot analysis. Five milliliters of induced cells was suspended in extraction buffer (10 mM Tris-HCl [pH 8.0], 1 mM EDTA, 100 mM NaCl, 2% Triton X-100, 1% SDS) and vortexed vigorously with glass beads in the presence of phenol-chloroform-isoamyl alcohol (25:24:1). Nucleic acid was precipitated from the aqueous phase with ethanol, redissolved, and digested with RNase A (43). RNA-free DNA (1.0 μg) was digested with EcoRI, fractionated by electrophoresis in a 0.8% agarose gel, transferred to a Duralon UV membrane (Stratagene, La Jolla, CA), and immobilized by UV cross-linking in a Stratalinker 1800 instrument (Stratagene). Hybridization was performed with a ^{32}P-labeled internal BglII fragment of Ty3, which hybridizes with the full-length 5.4-kbp Ty3 cDNA, as well as Ty3 donor plasmid and chromosomal Ty3 elements. The filters were washed and exposed to a Personal Molecular Imager FX phosphorimager screen (Bio-Rad Inc., Richmond, CA), and hybridization signals were quantitated by Quantity One software (Bio-Rad Inc.).

RNA protection assays. Yeast strain yTM443 was grown under conditions of Ty3 expression for 24 h. Five milliliters of induced cells was suspended in 100 μl of extraction buffer (100 mM KCl, 10 mM Tris-HCl [pH 7.5], 10 mM EDTA, 2.1 μg/ml aprotinin, 6.6 μg/ml pepstatin, 2 mM phenylmethylsulfonyl fluoride, 0.66 μg/ml leupeptin, and 5.3 U RNase inhibitor) and vortexed vigorously with sterile glass beads. An additional 150 μl of extraction buffer was added, and WCEs were cleared by centrifugation at 500 × *g* for 5 min at 4°C. WCEs were divided into three fractions of 65 μl each. In order to test for protection of genomic RNA, extracts were incubated with the nuclease benzonase. Ty3 control RNA was generated in vitro by T7 RNA polymerase transcription of a Ty3 template plasmid linearized at the downstream end of Ty3 by digestion with SnaBI. WCEs were processed by a modification of the benzonase assay previously described (59), except that 5 μg of in vitro-transcribed Ty3 RNA was added per reaction. Two of the fractions were incubated, one on ice and one at 24°C, with 15 μl of RNase-free benzonase buffer (100 mM Tris [pH 7.5], 100 mM $MgCl_2$) for 7 min. The third fraction was incubated at 24°C for 1 min, followed by the addition 5 μl of benzonase buffer and 36 U of benzonase and incubation for 6 min. The benzonase reaction was terminated by the addition of 5 μl of 0.5 M EDTA, followed by 300 μl of BSE buffer (10 mM Tris [pH 7.5], 10 mM EDTA, 2% SDS), and RNA was extracted with 300 μl of phenol-chloroform-isoamylalcohol (25:24:1). This extraction was repeated three more times, and the aqueous layer was precipitated with 2 volumes of ethanol. The pellet was resuspended in 25 μl of diethyl pyrocarbonate-treated water with 10 U of RNase inhibitor. Two microliters was denatured in 6.7% glyoxal for 1 h at 50°C and resolved by agarose gel electrophoresis in a 1% agarose gel in 10 mM sodium phosphate buffer (pH 7.0). The RNA was transferred to a Duralon UV membrane (Stratagene, La Jolla, CA) and immobilized by UV cross-linking in a Stratalinker 1800 instrument (Stratagene). Hybridization was performed with a ^{32}P-labeled internal BglII fragment of Ty3. Blots were processed as described previously (80).

Particle analysis by equilibrium gradient centrifugation and sedimentation. Conditions for fractionation of Ty3 VLP forms were derived empirically to maximize the separation of immature and mature VLP components (V. Bilanchone, unpublished data). In the protocol, cell extracts are prepared by lysis under nondenaturing conditions and are fractionated by centrifugation to equilibrium at 100,000 × *g* on 20% to 60% (wt/wt) sucrose gradients for 17 h at 4°C. Extracts of cells induced for short times (e.g., 2 h at 24°C) show Gag3 protein near the bottom of the gradient, as do extracts of cells expressing PR mutants that fail to process (V. Bilanchone, unpublished). Extracts of cells induced to express Ty3 for longer times (e.g., 6 h) show processed forms of Gag3 near the middle of the gradient. CA that is no longer associated with VLPs migrates at the top of these gradients.

YTM443 cells transformed with wt and representative mutant derivative Ty3 plasmids were induced for Ty3 expression by growth in galactose for 24 h at 24°C. Ten milliliters of induced cells was resuspended in 300 μl of STEK10 buffer (10% [wt/wt] sucrose, 10 mM Tris-HCl [pH 7.5], 10 mM EDTA, 100 mM KCl [pH 7.5]) with protease inhibitors (1 mM phenylmethylsulfonyl fluoride, 1 μg/ml pepstatin, 2.1 μg/ml aprotinin, 16 U RNase inhibitor) and vortexed vigorously with sterile glass beads. Three hundred microliters of cleared extract was fractionated by equilibrium sedimentation over a 20/30/60% (wt/wt) linear sucrose gradient by centrifugation in a SW55 Ti rotor at 100,000 × *g* for 17 h at 4°C. Fourteen 340-μl fractions were successively removed from the top of the gradient. For each fraction, 70-μl aliquots were used for protein analysis. The 70-μl aliquot of each fraction was trichloroacetic acid precipitated in the presence of 0.013% deoxycholate and fractionated by electrophoresis in a 4 to 20% SDS-polyacrylamide gel (Pierce Biotechnology Inc., Rockford, IL) for immunoblot analysis as described above.

In order to further test for particle formation, WCEs were subjected to velocity sedimentation. Cells of yeast strain yTM443 transformed with pDLC201 mutant derivative plasmids and the target plasmid pCH2vo19V were grown as described above for immunoblot analysis. WCEs from 5 ml of induced cells were prepared as described for RNA protection assays. Cleared WCEs were divided into two portions: one untreated and the other adjusted to a final concentration of 1% Triton X-100. Both were incubated for 10 min at 24°C, followed by centrifugation in a TLA 100.3 rotor at 100,000 × *g* for 30 min. Pellets were resuspended in equal volumes of supernatants, and fractions for both treated and untreated samples were fractionated by electrophoresis in a 4 to 20% SDS-polyacrylamide gel and analyzed by immunoblotting with anti-Ty3 CA and anti-Ty3 IN, as described previously.

Fluorescence microscopy. The proposed assembly site for Ty3 is the P body. The ability of different CA mutants to localize to the P body was therefore determined. Fluorescence microscopy of wt and mutant variants of Ty3-RFP in a strain in which the P body was visualized by the P-body marker protein Dhh1-GFP was as previously described (6). Induction of Ty3 expression was as described above for immunoblot analysis except that inductions were from 18 to 24 h. One hundred fifty cells representing each of two independent transformants were observed for 21 mutants that were defective for transposition and 2 that transposed at wt frequencies.

EM. Cells of yeast strain BY4741 transformed with pDLC201 or mutant derivative plasmids were grown in noninducing SR-Ura medium until early log phase, induced by the addition of galactose to 2%, and grown for 6 h at 24°C. Cells (12 OD units) were prepared for EM as described previously (89) except that cell walls were digested with 2 ml potassium phosphate buffer, 0.25 mg/ml Zymolyase 100T (U.S. Biological, Swampscott, MA), and 90 mM β-mercaptoethanol for 20 min at 30°C. Cells were imaged with a transmission electron microscope (H7600; Hitachi, Tokyo, Japan). Approximately 100 cells were observed per mutant transformant. Cells induced for this experiment were confirmed to have been induced and to have a pattern of protein expression consistent with previously described transformants by immunoblot analysis using anti-CA (data not shown).

TABLE 2. Ty3 CA mutant phenotypes[a]

Mutation(s)	CA processing	IN	cDNA/plasmid ratio	Transposition score (30°C/24°C)	% RNA protection	P-body localization	Group
None	wt	+	1.25 ± 0.31	+++/+++	33 ± 8	+	
K15A/E19A	Like wt	+	1.4	−/+	53	+	II
R33A/R35A/D37A	Doublet bands	−	0	−	ND	+	IV
K40A/K42A	Reduced	−	0	+/++	3	+	III
D60A/R63A	None	−	0	−	1	−	V
R68A/R69A	Doublet bands	−	0	−	ND	+	IV
D81A/E85A	Doublet bands	−	0	−	1	+	IV
E90A/D94A	Doublet bands	−	0	−	ND	+	IV
K106A/D109A	Doublet bands	−	0	−	ND	+	IV
E122A/K124A	Doublet bands	−	0	−	ND	+	IV
E128A/R129A	Like wt	+	1.2	+/+++	10	ND	III
R133A/R135A/K136A	Like wt	+	0.9	+++	ND	ND	I
D139A/R140A	Like wt	+	2.6	+/+++	22	ND	III
E148A/K149A	None	−	0	−	10	−	V
K161A/E162A	Like wt	+	0.7	+/+++	24	ND	III
K171A/E173A	Like wt	+	3.6	+++	55	+	I
K176A/D177A	Like wt	+	4.8	+++	48	+	I
E180A/E181A	Reduced	−	0	−	2	+	IV
E190A/R191A	Reduced	−	0	−	4	+	IV
E197A/D199A	Like wt	+	2.2	±/++	50	+	III
D201A/D203A	Like wt	+	2.8	+/++	66	+	III
Q86A (MHR1)	Like wt	+	2	+++	33	+	I
G87A (MHR2)	Reduced	−	0	−/+	2	+	IV
E90A (MHR3)	Like wt	+	2.6	++	89	+	III
F93A (MHR4)	Reduced	−	0	−/+	ND	+	IV
F96A (MHR5)	Doublet bands	−	0	−/+	1	+	IV
L100A (MHR6)	Reduced	−	0	−/+	ND	+	IV

[a] ND, not determined.

RESULTS

Ty3 CA structure model. A consensus approach was used to generate a secondary structure prediction for Ty3 CA. Predicted helical regions of Ty3 CA account for 58% of the entire sequence (Fig. 1C). This is comparable to the structure-based helical compositions of HTLV-1, RSV, EIAV, and HIV-1, which are 57%, 58%, 60%, and 63%, respectively (8, 10, 17, 20, 34, 35, 39, 48, 50, 51, 62, 63). In the case of each retrovirus CA, helices are separated into NTD and CTD by a flexible loop region. In Ty3 CA, a 7-aa loop region separates the predicted NTD (aa 2 to 139) and CTD (aa 148 to 207) helical clusters. No structure could be predicted for amino-terminal residues 7 to 17 and carboxyl-terminal residues 193 to 207. It is presumed that they are flexible or adopt multiple conformations. In this prediction, the Ty3 MHR spans a loop-helix junction in the NTD. This differs from the retroviral CA MHR, which overlaps the beginning of the CTD.

Ala-scanning mutagenesis strategy. Residues of Gag3 within hydrophilic surface patches potentially mediate interactions with other Gag3 molecules, genomic RNA, or host proteins that are important for VLP assembly. An Ala-scanning mutagenesis strategy was used to specifically address the roles of these residues in assembly (Fig. 1D). A total of 18 double and 2 triple mutants were generated, resulting in a total of 42 residues converted to Ala. In addition, the six conserved amino acids in the Ty3 MHR (residues 86 to 104) were individually converted to Ala. Mutants were characterized by transposition, immunoblot, Southern blot, RNA protection, equilibrium velocity gradient, particle sedimentation, fluorescence microscopy, and EM analyses. The properties of each mutant are summarized in Table 2.

Retrotransposition of Ala-scanning mutants. A qualitative genetic assay was performed to determine the effects of CA mutations on retrotransposition frequency (52) (Fig. 2; Table 2). Two independent transformants were tested for wt Ty3 and each mutant at 24°C and 30°C.

Four of the 26 mutants [R133A/R135A/K136A, K171A/E173A, K176A/D177A, and Q86A (MHR1)] had frequencies of transposition that were indistinguishable from that of the wt at both temperatures. Seven of the mutants displayed significant levels of transposition but were defective at one or both temperatures [K40A/K42A, E128A/R129A, D139A/R140A, K161A/E162A, E197A/D199A, D201A/D203A, and E90A (MHR3)]. Fifteen of the mutants were severely blocked for transposition at both temperatures [K15A/E19A, R33A/R35A/D37A, D60A/R63A, R68A/R69A, D81A/E85A, E90A/D94A, K106A/D109A, E122A/K124A, E148A/K149A, E180A/E181A, E190A/R191A, G87A (MHR2), F93A (MHR4), F96A (MHR5), and L100A (MHR6)]. Of the 18 mutants with mutations in the amino-terminal 140 residues of CA, 12 were severely disrupted for transposition. The strongest temperature dependence was observed for three mutants with Ala substitutions near the predicted interdomain loop region (E128A/R129A, D139A/R140A, and K161A/E162A).

Polyprotein processing. YTM443 transformants carrying pDLC201, the Ty3 expression plasmid, with wt Ty3 or mutant derivatives were grown in SR-Ura medium. Cultures were induced for Ty3 expression by the addition of galactose to 2%

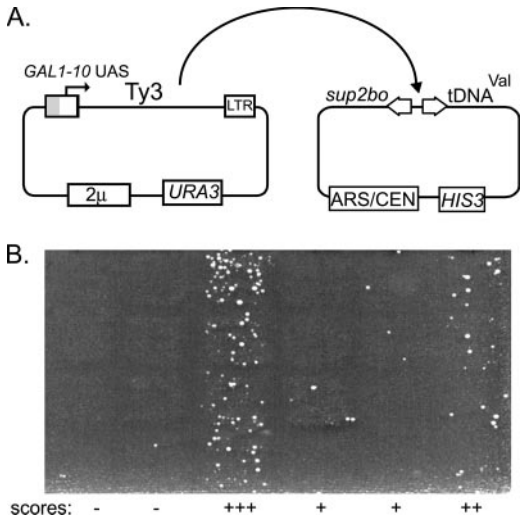

FIG. 2. Analysis of Ty3 retrotransposition. (A) Strategy. Ty3 and mutant variants were transformed into yTM443 and expressed on a high-copy-number *URA3*-marked plasmid. Transposition into the low-copy-number target plasmid activates expression of the *sup2bo* ochre suppressor required for growth on selective medium. LTRs are indicated as boxes; the *GAL1-10* UAS is indicated as a gray portion where it replaces part of the upstream LTR to confer galactose regulation. (B) Qualitative transposition assay. Activation of suppression by transposition into the target allows colony growth on minimal medium supplemented with Leu and Trp. Cells with transpositions become papillations on selective medium, and phenotype is scored for several independent mutants (−, ±, +, ++, and +++). Patterns are shown for a representative sample of mutants at 24°C.

(SG-Ura) and were grown for 24 h at 24°C. Proteins were extracted under denaturing conditions, and WCE were subjected to immunoblot analysis using antibodies against CA (Fig. 3A) or IN (Fig. 3B). Most mutants produced significant amounts of Ty3 protein, indicating that in most cases, Gag3 stability was not the only factor accounting for decreased transposition. In cells expressing Ty3 for long periods of time, during which they enter stationary phase, Gag3 also undergoes limited background proteolysis by cytoplasmic proteases to produce products similar in size to p27 and CA (data not shown). Therefore mutations that fully blocked PR activation could not be unambiguously identified. Nevertheless, the extent of Gag3 processing correlated well with the severity of mutant transposition phenotypes.

Extracts of cells expressing wt Ty3 and each of the four mutants with wt levels of transposition [R133A/R135A/K136A, K171A/E173A, K176A/D177A, and Q86A (MHR1)] showed similar amounts of Gag3 and p27 and a significantly greater amount of CA than either other species (Fig. 3A). These extracts showed similar amounts of IN (Fig. 3B).

Seven mutants showed significant, but attenuated, transposition at one or both temperatures [K40A/K42A, E128A/R129A, D139A/R140A, K161A/E162A, E197A/D199A, D201A/D203A, and E90A (MHR3)]. These mutants generally showed levels of CA approaching that found in wt and detectable IN. Only the mutant that was lowest for transposition (K40A/K42A) had amounts of Gag3 greater than CA and no detectable IN.

Fifteen mutants were severely reduced in transposition. Surprisingly, one of these (K15A/E19A) showed a wt pattern of protein maturation for Gag3 and IN. Fourteen mutants showed reduced or no Gag3 processing and no detectable IN. These mutants were differentiated into three classes based on the pattern of Gag3 and IN immunoblot analysis: (i) limited and aberrant processing (R33A/R35A/D37A, R68A/R69A, D81A/E85A, E90A/D94A, K106A/D109A, and E122A/K124A); (ii) severely reduced processing [E180A/E181A, E190A/R191A, G87A (MHR2), F93A (MHR4), F96A (MHR5), and L100A (MHR6)], and (iii) no detectable processing (D60A/R63A and E148A/K149A). Overall, based on inferences of apparent processing of Gag3, multimerization was robust. The extracts of mutants in the first and second classes generally had higher levels of Gag3 than were observed in extracts of cells expressing wt Ty3, suggesting that Gag3 was accumulating in a stable form. Only two mutants (D60A/R63A and E148A/K149A) showed Gag3 but completely lacked detectable smaller species. In contrast to extracts of cells expressing other mutants with severely reduced processing, which showed accumulation of Gag3, these extracts had amounts of Gag3 similar to extracts of cells expressing wt Ty3, consistent with reduced levels of expression or instability.

Based on the foregoing analysis of transposition and protein processing, mutants were classified as follows: group I, not measurably affected [R133A/R135A/K136A, K171A/E173A, K176A/D177A, and Q86A (MHR1)]; groups II and III, mod-

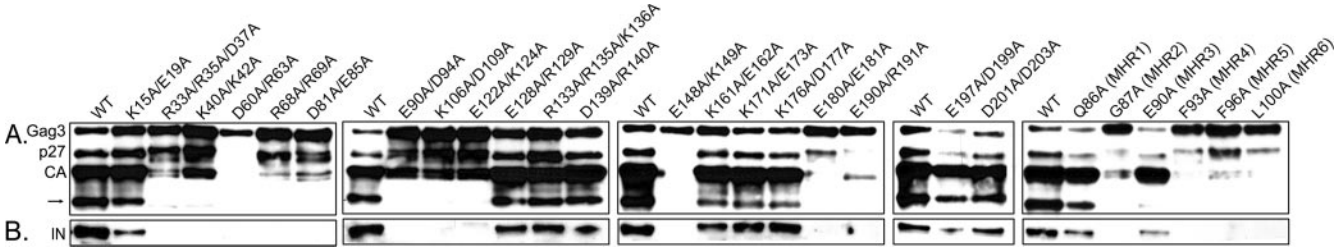

FIG. 3. Immunoblot analysis of Ty3 proteins in WCE. (A) Immunoblot analysis of Ty3 Gag3 proteins. Cultures were induced for Ty3 expression for 24 h at 24°C, and WCEs were prepared under denaturing conditions as described in Materials and Methods. Equivalent volumes of WCEs from cells expressing the indicated mutations were fractionated by electrophoresis on a 4 to 20% SDS-polyacrylamide gel and analyzed by immunoblotting using polyclonal anti-CA. The arrow indicates a lower-molecular-weight protein that appears at later times of expression. (B) Immunoblot analysis of Ty3 IN. WCEs were prepared and processed for immunoblotting as described for panel A except that polyclonal antibody against IN was used.

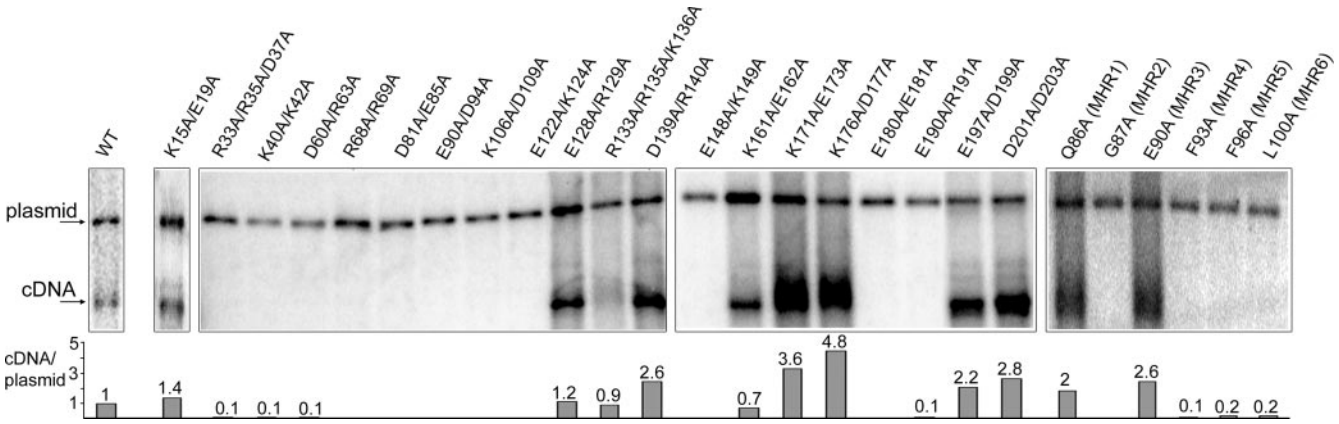

FIG. 4. Southern blot analysis of mutant Ty3 cDNA. Total nucleic acid was purified from cells induced for Ty3 expression as described in the legend to Fig. 3, and DNA was cleaved with EcoRI to linearize the Ty3 expression plasmid. Southern blot analysis was performed with a ^{32}P-labeled Ty3-specific probe, which hybridizes with the full-length 5.4-kbp Ty3 cDNA (cDNA), as well as with Ty3 donor plasmid (plasmid). The Ty3 cDNA/plasmid ratio for four independent wt cultures was 1.3 ± 0.3. Measurements were normalized to this ratio.

est to no detectable defects in protein processing [K15A/E19A, K40A/K42A, E128A/R129A, D139A/R140A, K161A/E162A, E197A/D199A, D201A/D203A, and E90A (MHR3)]; group IV, severely blocked prior to or during protein processing [R33A/R35A/D37A, R68A/R69A, D81A/E85A, E90A/D94A, K106A/D109A, E122A/K124A, E180A/E181A, E190A/R191A, G87A (MHR2), F93A (MHR4), F96A (MHR5), and L100A (MHR6)]; and group V, present in small amounts with no protein processing (D60A/R63A and E148A/K149A). Mutant K15A/E19A was later designated group II based on its normal processing and cDNA pattern, which indicated a later defect in transposition than appeared to be the case for the other mutants in group III.

Reverse transcription. Mutations in CA produced a wide range of Gag3 and Gag3-Pol3 processing phenotypes, and many mutants that displayed some processing were significantly attenuated in transposition. In order to further differentiate the effects of these mutations, Ty3 extrachromosomal cDNA was measured in cells induced as described above (Fig. 4). Group I mutants all produced cDNA. The group II mutant, which failed to transpose but displayed normal processing, had a cDNA-to-plasmid ratio in the same range as wt Ty3. The seven group III mutants had detectable cDNA, with the exception of mutant K40A/K42A, which also showed less Gag3 processing. None of the group IV or V mutants had detectable cDNA.

Overall, these results showed clear and parallel effects of mutations in CA on Gag3 processing and accumulation of reverse transcripts. As was observed for protein processing, clusters of mutations with similar effects on cDNA production appeared to define CA subdomains. Examples of mutations defining such subdomains were 12 mutations in the proximal domain of the NTD between residues 33 and 124 (negative for cDNA), 7 mutations between residues 128 and 177 (with one exception, positive for cDNA), E180A/E181A and E190A/R191A (negative for cDNA), and E197A/D199A and D201A/D203A (positive for cDNA). Overall, mutations that attenuated processing resulted in complete loss of cDNA. This is consistent with the drastic reduction in reverse transcription activity previously observed for a Ty3 PR catalytic mutant (53).

Complex formation. Mutants that produced no cDNA showed a range of processing phenotypes. In order to better correlate the protein processing phenotypes with assembly, extracts of cells expressing representative mutants from groups III to V were subjected to equilibrium gradient sedimentation analysis.

As expected, extracts of cells expressing wt Ty3 contained a mixture of immature and mature VLP forms. As with observations in previous experiments (unpublished data), Gag3 was distributed from a density of 1.13 mg/ml to 1.23 mg/ml (Fig. 5), whereas mature CA was more concentrated, from 1.13 to 1.16 mg/ml. This region of the gradient is presumed to include mature VLPs. The group III mutant [E90A (MHR3)], which was transposition competent, showed a pattern very similar to that found in cells expressing wt Ty3.

The seven group IV mutants, which were severely reduced in transposition, protein processing, and amount of cDNA, showed patterns on the equilibrium gradients similar to those of a PR catalytic site mutant, which has been shown to be competent to assemble particles (55). This pattern was also similar to that of immature particles observed in extracts of cells expressing Ty3 for only 2 h (unpublished data). Immunoblot analysis of cells expressing mutant E180A/E181A (Fig. 5) showed a peak of Gag3 in the bottom-most fraction, with detectable amounts extending upward in the gradient. Mutant E190A/R191A also showed the greatest amount of Gag3 in the bottom of the gradient but in addition showed small amounts of processed forms in the same region as CA in extracts of cells expressing wt Ty3. Interestingly, extracts of the four MHR mutants in this group, which were among the most severely attenuated for protein processing, showed that mutant Gag3 accumulated at densities similar to those of immature wt particles.

The two group V mutants showed only Gag3, indicating that they failed to process and suggesting that they were potentially defective in some early aspect of particle formation. In the equilibrium gradient, Ty3 protein was undetectable in the lysates of cells expressing D60A/R63A (data not shown). Gag3 was also not detected in the pellet of the low-speed clarification spin that preceded gradient analysis (data not shown). Extracts of cells expressing the other group V mutant, E148A/

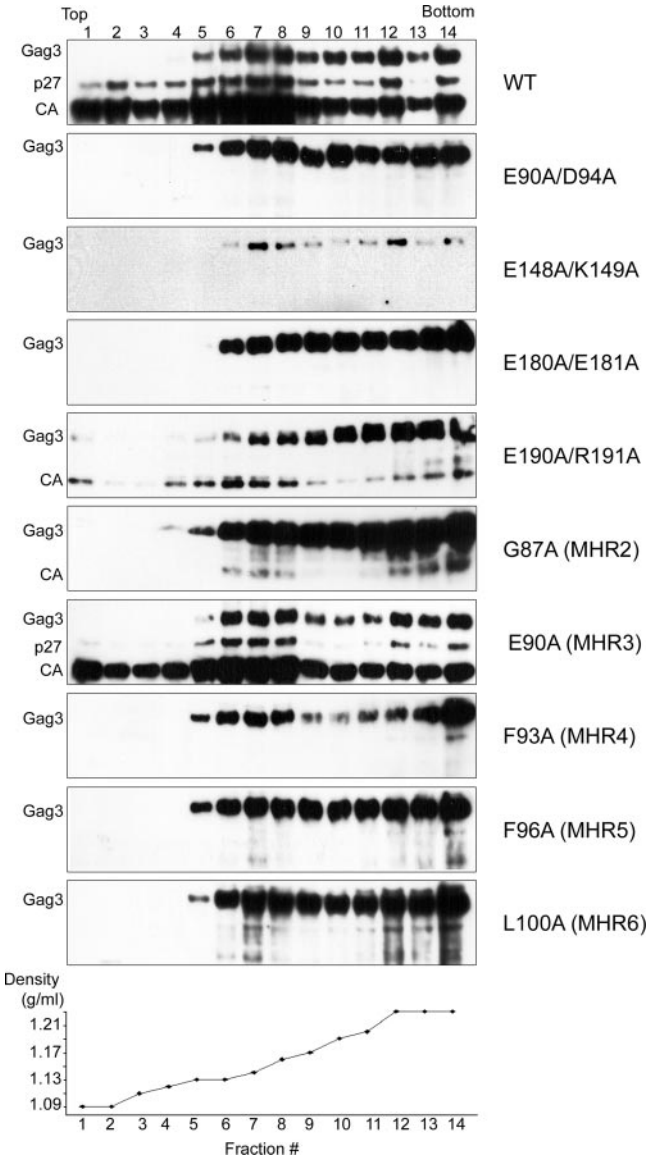

FIG. 5. Equilibrium gradient analysis of Ty3 wt and representative mutant WCEs. Cultures were induced for Ty3 expression as described in the legend to Fig. 3. WCEs were prepared under native conditions as described in Materials and Methods and were fractionated over a 20 to 60% (wt/wt) linear sucrose gradient and centrifuged to equilibrium. Fourteen 340-μl fractions were collected and examined by immunoblot analysis using anti-CA, as described in the legend to Fig. 3.

K149A, showed very small amounts of Gag3 precursor migrating similarly to Gag3 in wt particles (Fig. 5).

Equilibrium gradient centrifugation profiles of WCEs of cells expressing wt and group III, IV, and V mutants suggested that most or all were able to form particles. Although equilibrium gradient analysis showed that mutant Gag3 could be sedimented, it was possible that it was not particulate but associated with cellular membranes, causing it to sediment. In order to investigate this possibility, production of pelletable material in the presence and absence of detergent was also tested. WCEs obtained under nondenaturing conditions from cells expressing representative group IV and V mutants [E148A/K149A, E190/R191A, G87A (MHR2), F93A (MHR4), and F96A (MHR5)] were incubated in the presence or absence of 1% Triton X-100 and centrifuged at 100,000 × *g* for 30 min. In all cases examined, Ty3 Gag3 species sedimented, indicating that sedimentation was not Triton-soluble membrane dependent (Fig. 6). Examination of pellets and supernatants for Gag3-Pol3-related species using anti-IN antibody showed that processed IN was present in significant amounts only in the wt. Much lower amounts of partially processed Gag3-Pol3 species were present in the extracts of cells expressing each of the three MHR mutants (Fig. 6). Extracts of cells expressing E148A/K149A and E190A/R191A showed no detectable Gag3-Pol3 (IN)-related species.

Protection of genomic RNA. Gradient analysis indicated that most mutants were probably competent for some level of particle formation but did not differentiate among them with respect to particle integrity. Benzonase is a nuclease that degrades RNA and DNA. Genomic RNA of Tf1 retrotransposon VLPs was previously shown to be protected against benzonase digestion, making resistance to digestion an indirect measure of packaging (59). Wt Ty3 and Ty3 PR mutant (immature) VLPs have been similarly shown to protect Ty3 RNA (unpublished data). The benzonase protection assay was used to monitor Ty3 genomic RNA packaging.

Lysates of cells expressing wt or mutant Ty3 were supplemented with control in vitro-generated Ty3 transcripts and treated with benzonase as described in Materials and Methods. Nucleic acid in these extracts was analyzed by Northern blotting using a Ty3-specific probe. Under these conditions, 33% (± 8%) of wt Ty3 RNA was protected from benzonase digestion compared to untreated control extracts incubated on ice or at 24°C. Control in vitro Ty3 transcripts added to the cell extracts were completely sensitive to degradation (Fig. 7). A subgenomic 3.1-kb Ty3 RNA was previously reported (9) and was also observed in these experiments. It showed a pattern of protection similar to that of the genomic Ty3 RNA. However, it fractionated with mobility similar to that of 25S rRNA, which is degraded in the incubation. This loss of RNA in the same region of the gel affected the mobility and efficiency of filter transfer of the associated Ty3 RNA and made its measurement less accurate (data not shown).

Eighteen mutants representing groups I to V were tested for protection of Ty3 RNA from benzonase digestion (Fig. 7 and Table 2). The group I mutants tested [K171A/E173A, K176A/D177A, and Q86A (MHR1)] showed protection of RNA from 33% to 55%, the group II mutant (K15A/E19A) showed 53% protection, and group III mutant [E90A (MHR3)] showed 89% protection. These results were consistent with the ability of these mutants to produce cDNA. The K40A/K42A mutant, which showed the least transposition and the most-defective Gag3 processing pattern of the group III mutants and no detectable cDNA, showed only 3% protection. The five group IV mutants that were tested (including two MHR single-substitution mutants) showed protection of only 1% to 4% of the Ty3 RNA. This result was consistent with the severe defect in transposition and the uniform absence of detectable cDNA for cells expressing group IV mutants. The two group V mutants, which were the most severely affected by all other criteria, were also defective in genomic RNA protection. Mutant D60A/R63A protected 1% of the Ty3 RNA and mutant E148A/

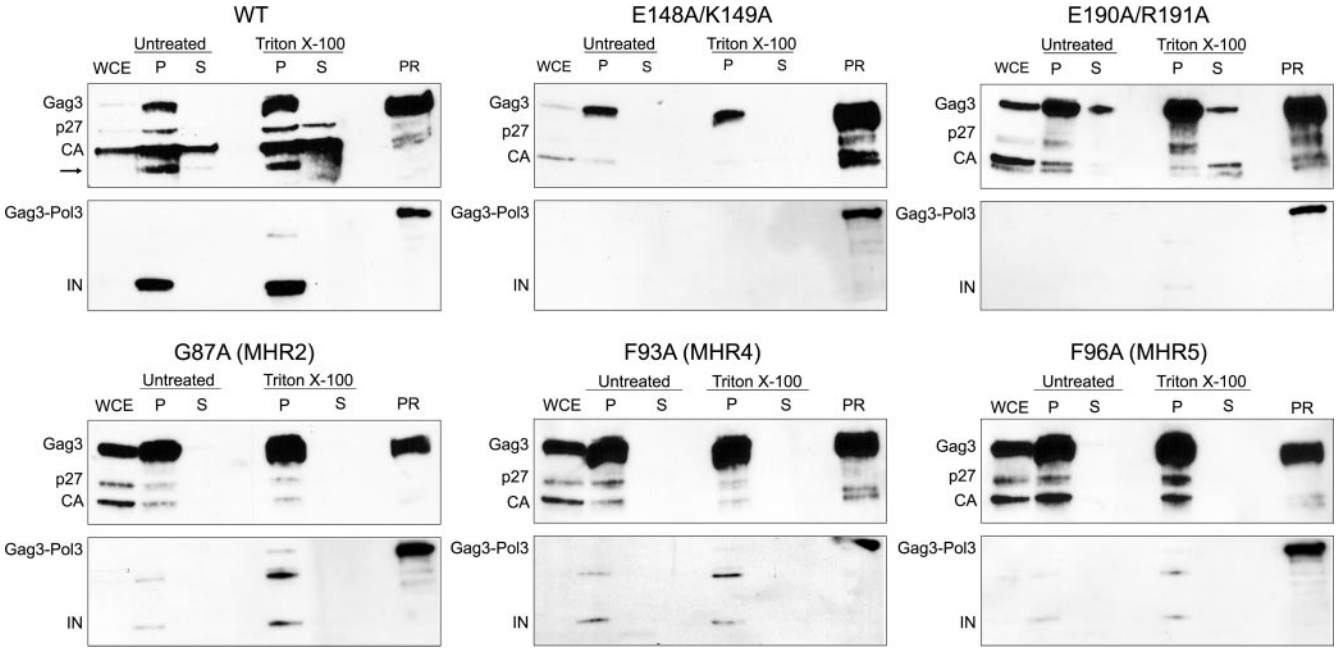

FIG. 6. Particle formation by representative mutants. Cells were induced and WCEs were prepared as described in the legend to Fig. 5. Aliquots of extracts were either analyzed directly or mixed with Triton X-100 for a final concentration of 1%. Extracts were analyzed by immunoblotting using anti-CA and anti-IN as described in the legend to Fig. 3. PR, similar amounts of extracts of a Ty3 PR catalytic site mutant which also produces substantial amounts of Gag3-Pol3 fusion protein. The arrow indicates a 17-kDa protein that appeared at later times in extracts of the wt and transposition-competent mutants.

K149A protected 10% of the RNA. These results showed a strong correlation between the ability of particles to protect genomic RNA and the presence of cDNA.

Northern analysis of untreated RNA samples showed that less RNA was recovered in the case of group V mutants D60A/R63A and E148A/K149A than for the other mutants. Investigation of localization of Ty3 proteins (see below) showed that a smaller proportion of cells was positive for expression of these mutants than for the wt. However, the proportion was similar to that for some other mutants that produced substantial amounts of RNA (data not shown). RNA was also extracted under denaturing conditions from cells expressing these mutants, and Northern analysis confirmed that Ty3 RNA was reduced (data not shown). Overall, group V mutants had reduced RNA and Gag3 protein and defective packaging.

Localization of assembly. Ty3 RNA, protein, and VLPs concentrate in association with P-body components (6). We have proposed that Ty3 assembles in association with P bodies, potentially as a mechanism for sequestering RNA packaging from translation. In order to test for a role for CA in Ty3 localization to P bodies, fragments containing 21 CA mutations representing groups I to V were swapped into Ty3-RFP and expressed under control of the *GAL1-10* UAS from a high-

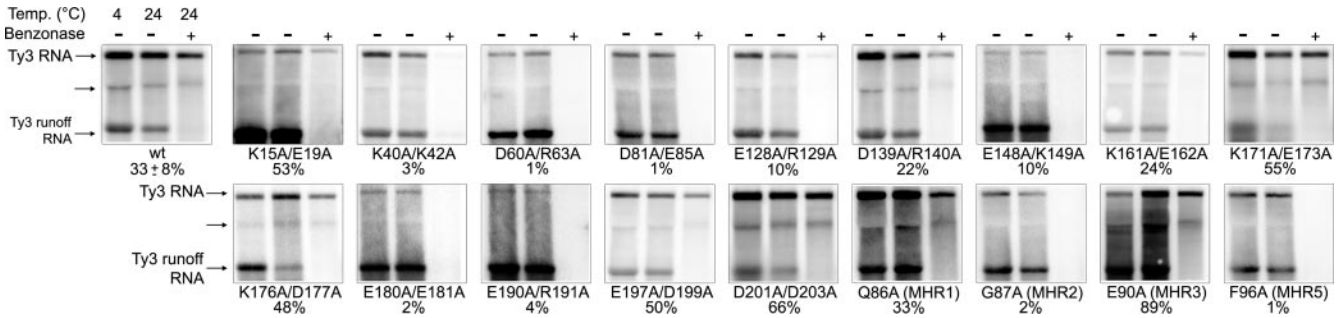

FIG. 7. Assay for protection of Ty3 genomic RNA in cells expressing the wt and CA mutants. Cultures were induced for Ty3 expression as described in the legend to Fig. 3, and WCEs were prepared under native conditions as described in the legend to Fig. 5. Positive control in vitro-transcribed Ty3 RNA (Ty3 runoff RNA) was added to each WCE. Untreated control samples were maintained at 4°C and at 24°C for 6 min (lanes 1 and 2, respectively, in each set). WCEs were treated with benzonase for 6 min at 24°C as described in Materials and Methods (lane 3 in each set). RNA was extracted and analyzed by Northern blotting using a ^{32}P-labeled Ty3-specific probe. Two or more independent experiments were performed for each mutant, and a representative example is shown. Ty3-related 3.1-kb RNA is indicated by the unlabeled arrow. Percent protection of RNA is indicated under each set.

copy-number plasmid (6). In this context, RFP is produced fused to the Ty3 IN domain. This fusion does not grossly interfere with assembly or Gag3 processing, and an IN-RFP fusion of the expected size is produced (6). Cells were induced for expression of Ty3-RFP or mutant derivatives for 24 h at 24°C. Protein was extracted, and immunoblot analysis was performed with anti-CA and anti-IN. This analysis showed that maturation of Gag3 and IN-RFP species in the Ty3-RFP derivative mutant was similar to that observed for Gag3 and IN, respectively, as observed for the untagged Ty3 mutant, except that the presence of low-mobility Gag3-Pol3-RFP species could not be assessed for mutants with little or no processing (data not shown). P-body localization was monitored as described previously by using a GFP reporter fused to the P-body protein Dhh1 (6, 86).

The 21 Ty3-RFP mutants were induced for 18 to 24 h at 24°C, and Ty3-RFP was localized relative to Dhh1-GFP for two independent transformants of each mutant (Fig. 8 and data not shown). Under these conditions, Ty3-RFP and Dhh1-GFP typically localize to a single large focus per expressing cell. Localization was determined for three of the four group I mutants [K171A/E173A, K176A/D177A, and Q86A (MHR1)]. Each produced a pattern of Ty3-RFP and Dhh1-GFP indistinguishable from that observed for the wt (Fig. 8 and data not shown). The late-acting group II mutant (K15A/E19A) also showed a pattern of Ty3-RFP and P-body fluorescence similar to that in cells expressing wt Ty3-RFP (Fig. 8).

Three group III mutants were examined. Mutant K40A/K42A, which was defective in protein processing and RNA protection, showed enlarged and faint RFP foci, which colocalized with Dhh1-GFP (data not shown). The other two group III mutants [E197A/D199A and E90A (MHR3)], which showed wt processing and 50% and 89% protection of RNA, respectively, were similar to wt Ty3-RFP in colocalization with the P-body marker protein (data not shown). These mutants all showed amounts of IN-RFP fusion protein similar to that observed in cells expressing wt Ty3-RFP (data not shown).

Inspection of all 12 group IV mutants with severely reduced, aberrant patterns of processing and little or no transposition showed differing patterns in Ty3-RFP. In some cases, even among transformants of a single mutant, there was a range of phenotypes. Mutant R33A/R35A/D37A showed large, faint clusters of Ty3-RFP. Mutant K106/D109A showed normal-sized, faint clusters, as well as some cytoplasmic fluorescence. Clusters in both cases colocalized with Dhh1-GFP (data not shown). Other group IV mutants (R68A/R69A, D81A/E85A, E90A/D94A, K106A/D109A, E122A/K124A, and E180A/E181A) showed more diffuse cytoplasmic RFP (e.g., Fig. 8, E90A/D94A, and data not shown). Even some group IV mutants that showed unusually diffuse patterns retained subsets of cells that showed colocalization of Ty3 and P-body markers. For example, Ty3-RFP and Dhh1-GFP formed elongated, polar foci in subpopulations of cells expressing the group IV mutants R68A/R69A, E90A/D94A, and E180A/E181A (data not shown).

A significant fraction of cells expressing mutant E190A/R191A showed colocalization of Ty3-RFP with Dhh1-GFP in a remarkable network of streaks (Fig. 8). Dhh1 is a candidate protein for shuttling of RNA into P bodies (11, 22). Thus, it was possible that Dhh1-GFP was somehow diverted away from P bodies in cells expressing this mutant. In order to investigate this possibility, a second strain, in which P bodies were labeled with Xrn1/Kem1-GFP, was used to express E190A/R191A (86). The resulting pattern was similar to that observed with Dhh1-GFP (data not shown). These results suggested that overexpression of aberrant Ty3 Gag3 causes relocalization of P-body components.

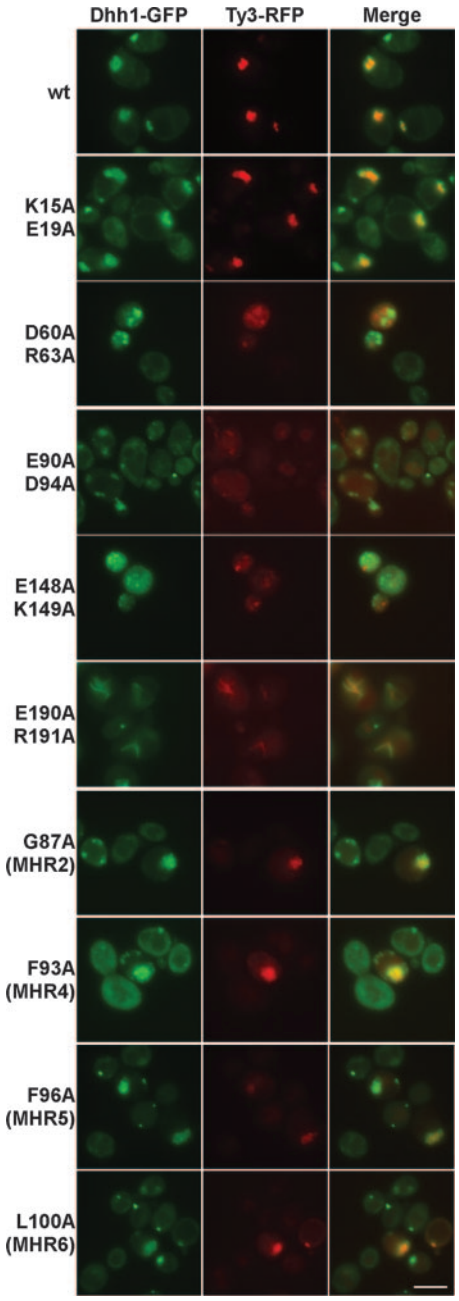

FIG. 8. Visualization of wt and mutant Ty3 and P bodies. CA mutations were introduced to Ty3-RFP and expressed in a strain that expresses a Dhh1-GFP marker under the native promoter. Mutants shown are representative of two independent transformants of each type. Cells were induced for 18 to 24 h as described in the legend to Fig. 3 (6). The scale bar at the lower right represents 5.0 μm.

The four single MHR replacement mutants [G87A (MHR2),

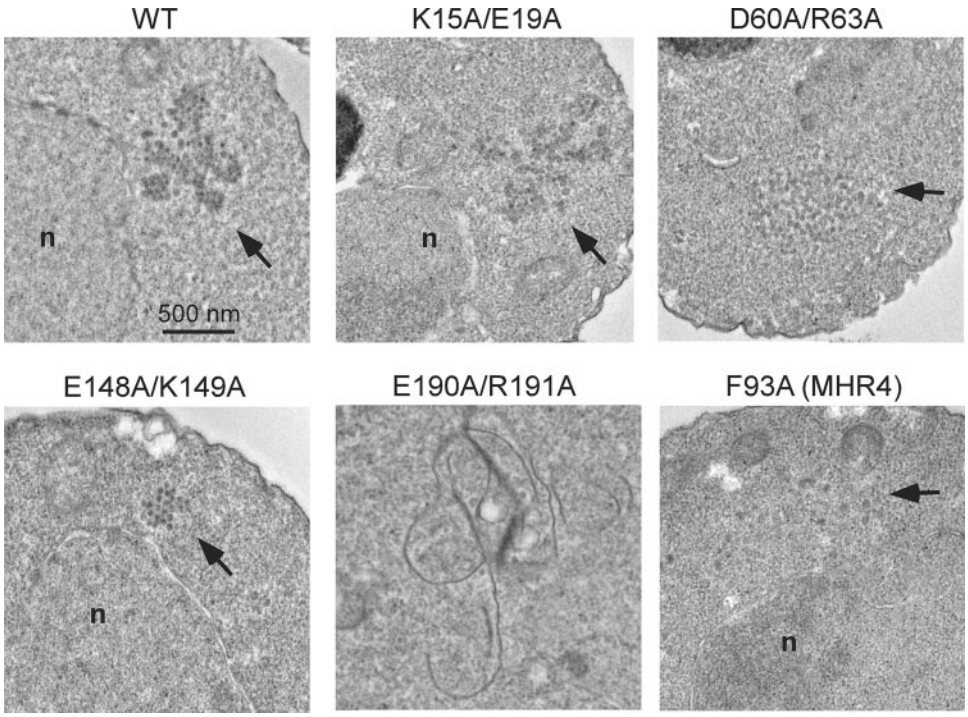

FIG. 9. EM of cells expressing Ty3 CA mutants. Cells transformed with the wt and Ty3 mutants K15A/E19A, D60A/R63A, E148A/K149A, E190A/R191A, and F93A (MHR4) were grown to log phase and induced for Ty3 expression for 6 h. Cultures were processed as described in Materials and Methods. Cells were imaged at 100 kV and ×5,000 direct magnification.

F93A (MHR4), F96A (MHR5), and L100A (MHR6)] formed a distinctive subset. They showed particulate material according to one or both of the sedimentation tests, but they were the most severely defective in protein processing of the group IV mutants. These mutants produced what in some cases appeared to be enlarged Ty3-RFP clusters, which colocalized with the P-body marker, or diffuse red fluorescence. In one case [F93A (MHR4)], there was even diffuse Dhh1-GFP fluorescence in addition to Dhh1-GFP colocalization with RFP (Fig. 8 and data not shown).

Cells expressing group V mutant Ty3-RFP showed low levels of red fluorescence in foci (e.g., Fig. 8, D60A/R63A and E148A/K149A). The low level of fluorescence was consistent with the low level of Gag3 observed with immunoblot analysis. The Dhh1-GFP pattern of multiple small foci in the cells expressing these mutants resembled the pattern in cells not expressing Ty3 (6). In addition, the green and red fluorescence foci did not overlap.

Electron microscopy of cells expressing Ty3 mutants. Group IV and V mutants failed to process Gag3 and showed variable patterns of localization, indicating defects in particle assembly. However, most mutant proteins separated from soluble protein fractions in equilibrium sedimentation and pelleting assays. Thus, it was possible that Ty3 proteins were associated with some larger structure or formed defective particles. In order to differentiate these possibilities, EM of cells expressing wt Ty3 and representative mutants was undertaken. Expression of wt Ty3 results in multilobed clusters of ~50-nm VLPs (Fig. 9) (41). Cells expressing the late-acting group II mutant K15A/E19A produced particles, but these were more loosely associated than were wt particles (Fig. 9 and data not shown). Group IV mutant E190A/R191A, which showed some processing but no cDNA synthesis, formed bizarre filamentous structures (Fig. 9 and data not shown). These structures were consistent with what was observed by fluorescence microscopy with the RFP-tagged Ty3 mutant. MHR mutants G87A (MHR2) and F93A (MHR4) were both severely deficient in processing and had no detectable cDNA. Fluorescence microscopy showed that G87A (MHR2) formed some clusters but that F93A (MHR4), in addition, had a considerable amount of cytoplasmic fluorescence. Equilibrium gradient analyses showed the presence of sedimentable material. Examination of over 100 cells expressing these mutants (Fig. 9 and data not shown) showed no cells with particles similar to those of the wt but a number of cells with regions containing a low concentration of particle-like structures, which appeared to be in a ribosome-free area. Although this was a negative result, it suggested that these MHR mutants are defective in particle formation. Group V was severely affected by the criteria of protein production, processing, and RNA protection and did not colocalize with P bodies. Only mutant E148A/K149A produced sufficient protein to be readily analyzed by sedimentation, and it showed sedimentable material. Both mutant D60A/R63A and mutant E148A/K149A produced small clusters of particles. Particles produced by expression of the former mutant appeared more heterogeneous, while those of the latter mutant were relatively uniform and compact (Fig. 9 and data not shown). Thus, surprisingly, group V mutants were found to be competent to assemble particle structures.

DISCUSSION

The secondary structure of the Ty3 CA protein was predicted by a consensus of several structure prediction algorithms to be similar to retroviral CA protein in that it is rich in α-helical structure. In order to understand CA subdomain functions, 22 Ala substitution mutants defective in transposition were characterized. Mutants were divided into five groups based on CA function. Four mutants (group I) were similar to the wt. One mutant (group II) was wt in Gag3 processing, RNA protection, and cDNA production but failed to transpose, indicating that the requirement for Ty3 CA function occurred after reverse transcription. Seven mutants (group III) had intermediate transposition phenotypes. This group was heterogeneous in biochemical properties. Twelve mutants (group IV), including four MHR single-substitution mutants, showed no transposition, severe reductions in Gag3 processing, and no cDNA. Representative mutants formed defective particles that did not protect genomic RNA. Localization of these mutants suggested that they were arrested in particle morphogenesis through different mechanisms. Two mutants (group V) produced small amounts of Gag3 and were defective by most criteria. Particle production was minimal or nonexistent.

In our study, residues and subdomains of Ty3 CA that contributed to localization of Ty3 components, integrity of RNA packaging, fidelity of protein processing, reverse transcription, and post-reverse transcription stages of transposition were identified. However, this analysis showed that particle formation per se is relatively resistant to mutations in CA and that multiple Gag3 domains are therefore likely to be involved.

Prediction of the Ty3 CA tertiary structure. In order to better relate the outcome of our mutagenesis study to what is known about the structure and function of retrovirus CA, a tertiary structure was predicted for Ty3 CA. A protein threading approach (see Materials and Methods) and the known structures of HTLV-1 (50), HIV-1 (8, 20, 63), EIAV (10), and RSV (17) were used to generate this prediction. The predicted Ty3 CA has a large bundle of seven α helices in the NTD separated from a smaller CTD bundle by an unstructured loop (Fig. 10). As in the case of retroviruses, a disparity in volume of the predicted CA domains could contribute to curvature of the mature VLP surface. The position of the Ty3 MHR overlapped a loop-helix junction in the Ty3 CA NTD. It differs from the position of the retroviral MHR, which overlaps the NTD-CTD junction and the first helix of the CTD. The threading prediction differed from the secondary structure prediction in the terminal regions. This may indicate that these regions can adopt more than one conformation.

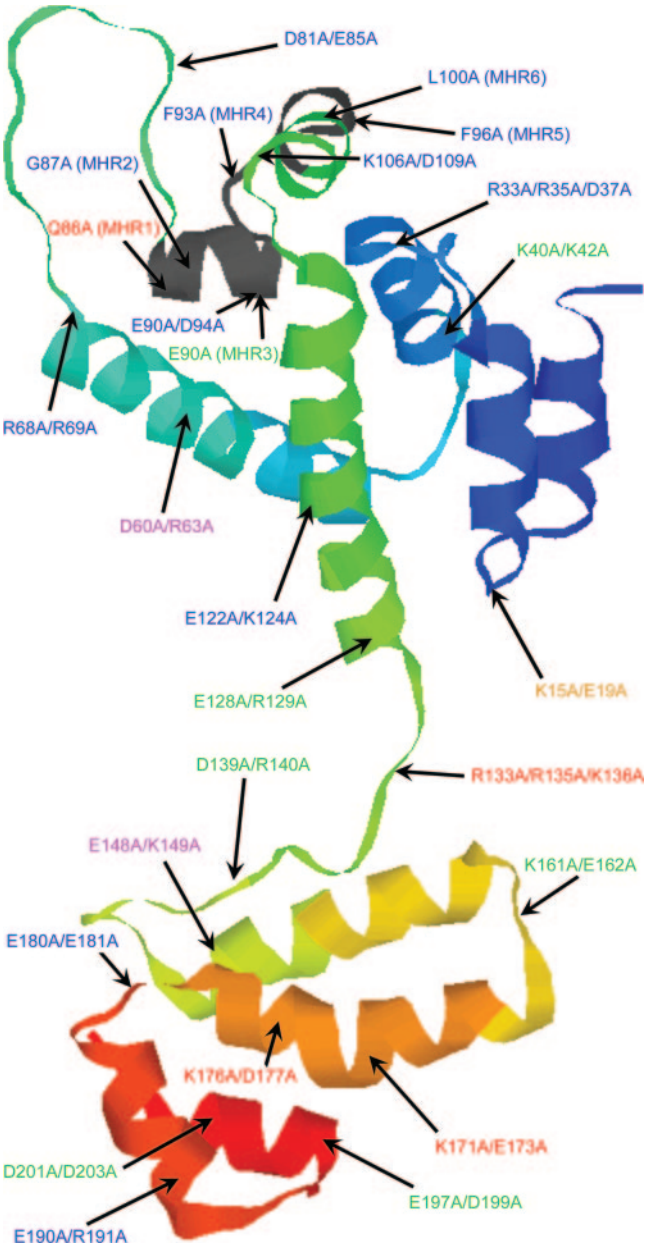

FIG. 10. Ribbon representation of modeled tertiary structure of Ty3 CA. The predicted Ty3 CA tertiary structure is comprised of NTD and CTD bundles of seven and four α helices, respectively. Mutations indicated in the modeled structure are color coded according to the mutant phenotype group (see Table 2). In order of least to most deficient: group I (red), group II (ochre), group III (blue), group IV (blue), and group V (fuschia).

Localization of VLP assembly. Cells expressing Ty3 colocalize Ty3 and P-body components. Because Ty3 lacks a discrete MA domain and because CA is important for particle function, we hypothesize that CA drives localization of Ty3 components.

Mutations in CA had diverse effects on colocalization of VLP and P-body components. Mutants in group IV, none of which displayed significant transposition, were mostly of two types: those that formed large Ty3-RFP-Dhh1-GFP foci and those that showed diffuse cytoplasmic RFP. Five group IV mutants had mutations that affected localization of the P-body marker, including three mutants that showed cells with elongated cap-like structures or streaks of RFP and GFP and one MHR mutant that showed more diffuse cytoplasmic GFP than did the wt. These mutations indicate that the colocalization of Ty3 VLP and P-body components is based on physical interactions. This study did not indicate whether those interactions are direct or indirect.

Cells in which group V mutants were expressed showed multiple small Dhh1-GFP foci, typical of cells not expressing Ty3. Strikingly, the RFP Ty3 marker of the group V mutants

was present in smooth round foci, which did not colocalize with the Dhh1-GFP marker, and potentially represented sequestration of Ty3-RFP or RFP alone in some vesicular compartment. In order to examine this possibility, cells were stained with a fluorescent lipophilic dye, FM4-64 (92). Because FM4-64 fluoresces in the red wavelength overlapping RFP, group V mutations were individually introduced into Ty3-GFP. Cells expressing either group V mutant for 6 h showed a severely retarded endosomal uptake of dye. A previous screen of the yeast knockout collection showed that several ESCRT trafficking components contribute positively to Ty3 transposition (45). One possibility is that Ty3 Gag3 normally interacts transiently with a trafficking component and that this interaction is disrupted in the case of the group V mutant Gag3, thus interfering with function of a trafficking factor.

Examination of these cells by EM showed that Ty3 particles occurred in clusters similar to what was suggested by the fluorescence study. This result implicates the CA domain in colocalization with P-body components, as opposed to a model in which P-body colocalization is solely determined by Ty3 RNA. In addition, this result argues against the possibility that P-body components are needed simply for multimerization of particles.

Results of the present study argue that (i) Ty3 can multimerize prior to or in the absence of P-body localization, (ii) the CA domain of Gag3 contributes to typical P-body colocalization and may even interact directly with P-body components, and (iii) Gag3 localization to P bodies is not sufficient to guarantee protection of genomic RNA. We failed to observe mutants that did not associate with the P-body marker and were transposition competent. Thus, our results are consistent with, but do not demonstrate a role for P-body association in, Ty3 VLP assembly.

Even if Ty3 is shown to assemble in P bodies, the overall impact of P-body association on transposition is likely to be complex. The extent to which cells overexpressing Ty3 accumulate VLPs within a single cluster suggests that this structure could become limiting for transposition. We speculate that this phenomenon contributes to copy number control, which has been described for Ty1 (24) and also occurs for Ty3 (unpublished observations).

Because retrovirus targeting to assembly sites is specified by MA and envelope, the extent to which our findings bear upon retrovirus assembly and CA function in particular is not clear. However, similar to our results, recent studies of retroviral assembly have shown that intracellular complexes smaller than cores form prior to budding from the assembly site (56, 91). It is even possible that there is some specialization in these preassembly multimerization sites. For example, HIV-1 passes through a perinuclear compartment prior to delivery to the multivesicular body (71). Whether that compartment is related to the P body is not known; however, APOBEC3G, a host restriction factor for HIV-1, was recently reported to localize to P bodies (97). It has also been reported that the endogenous retrovirus related to Jaagsiekte sheep retrovirus and the endogenous musD mouse retrovirus accumulate Gag proteins at intracellular foci (66, 75).

Structural role of CA in VLP assembly. Particle production was observed for Ty3 CA mutants representing each group. Thus, it could be that multiple subdomains of CA or other domains of Gag3, such as spacer and NC, make important contributions to multimerization. In contrast, Ty3 particle function was relatively sensitive to mutation. Interestingly, 12 of 18 Ty3 CA NTD mutants had reduced particle functionality. The extreme amino-terminal group II mutant (K15A/E19A), which produced cDNA but failed to transpose, was among these. Additional mutagenesis has shown that individual substitutions at positions 15 and 16 affect clustering and assembly, respectively, further supporting a key role for the NTD in Ty3 VLP assembly (unpublished observations). Consistent with the NTD interface of the hexameric retrovirus CA, Ala-scanning mutagenesis of HIV-1 CA showed that the NTD influences the shape and stability of cores and may even influence nuclear entry (27, 31, 37).

The Ty3 MHR is located in the NTD rather than at the NTD-CTD junction, as occurs in retrovirus CA. Therefore, differences between MHR functions in retrovirus and Ty3 particle assembly may exist. Depending on the severity of the mutation, disruption of the MHR can cause defects in particle formation, infectivity, and cDNA synthesis (16, 28, 60, 88). At the mechanistic level, the MHR has been implicated in membrane association (29), incorporation of Gag-Pol into particles (44, 87), and productive assembly of Gag (72). It has been suggested that the MHR exerts its effect on assembly by mediating a CTD swap, which stabilizes a dimer interface (46).

In a previous study, we mutated three of the six conserved positions in the Ty3 MHR (aa 86, 87, and 90). The results of that study were consistent with the results of this study in that the effects of substitutions at aa 86 (Q86R) and 90 (E90D, E90K, and E90N) were less severe than at aa 87 (G87A and G87V). The present study showed that some MHR mutants, which are defective in protein processing and transposition, do localize to P bodies. However, at least one had a more cytoplasmic localization. In addition, our data suggest that at least some residues in the MHR are critical for assembly or stability of particles. Two of the severely defective mutants that were examined by EM (G87A and F93A) were decreased in VLP formation, consistent with defects in RNA protection. In addition, although MHR mutant Gag3 appeared to be stable, Gag3-Pol3-derived IN was reduced or absent in extracts of cells expressing MHR mutants and the ratio of Gag3-Pol3 to Gag3 species in pelletable material was severely reduced. Since at least one mutant competent for cluster formation was nonetheless defective in particle assembly by EM, these results suggest that the MHR could participate in more than one phase of particle assembly.

The group V mutant D60A/R63A is mutated at a position similar to the Asp that is conserved among retrovirus CA proteins and which participates in a salt bridge with a conserved amino-terminal Pro residue after Gag maturation. Replacement of this residue has been shown to destabilize retrovirus cores. Although Ty3 does not have an amino-terminal Pro, it is possible that the Asp at position 60 of the Ty3 CA performs a similar stabilization function. The group V mutant (E148A/K149A) bridges the NTD-CTD loop and the first CTD helical region. This is the position of the MHR in retroviral CA. The fact that mutations in conserved residues of the MHR, as well as mutations in the NTD-CTD linker, have effects on transposition suggests that functions performed by the MHR linker in retrovirus CA could be contributed by

separate subdomains in Ty3 CA. Specifically, the MHR in Ty3 CA could not participate in a CTD dimer swap, as proposed by Ivanov et al. (46).

The two group V mutations dramatically reduced the steady-state levels of Ty3 RNA and protein and disrupted processing. Although formally we cannot exclude the possibility that Gag3 plays a dual role by acting as a genomic RNA export factor, similar to that proposed for RSV Gag (15, 83), we think that the primary defect in these mutants is in Gag3 protein. After 2 h of expression of wt and group V mutant Ty3 elements, cell extracts show similar amounts of Gag3 (data not shown). Mutant Gag3 simply fails to accumulate either in processed form or in precursor form (as it does in other mutants). As production of new RNA declines at later times in the culture, RNA could be destabilized relative to wt Ty3 RNA due to disruption of packaging. Group V mutants fail to localize to P bodies and fail to form particles efficiently.

Two CTD mutants (E180A/E181A and E190A/R191A) displayed no transposition. Expression of mutant E180A/E181A resulted in some cytoplasmic Ty3-RFP, but also localization to cell poles, reduced amounts of Gag3 and Gag3 processing, and undetectable protection of genomic RNA. The E190A/R191A mutant also had reduced protein levels, minimal protein processing, and undetectable protection of genomic RNA. This mutant displayed an aster-like pattern of Ty3-RFP and Dhh1-GFP reminiscent of cytoskeletal elements. One possibility was that cytoplasmic trafficking of Ty3 RNA was disrupted in this mutant and RFP and GFP were displayed along the cytoskeleton. However, fluorescence microscopy using phalloidin A to stain actin or anti-tubulin antibodies and fluorescent secondary antibodies showed that these cytoskeletal markers did not colocalize with Ty3 or P-body markers (data not shown). EM analysis of mutant E190A/R191A showed a filamentous structure. If, similar to what has been proposed for retroviruses, the Ty3 CA CTD forms interhexamer contacts, increasing or decreasing the affinity of those interactions could change the kinetics of assembly, resulting in aberrant structures. Mutations in the carboxy-terminal 11 aa of Ty3 CA did not produce strong phenotypes.

Post-reverse transcription requirement for CA. In fungi, the nuclear envelope does not disintegrate during mitosis. It is speculated that under these conditions, Ty3 core particles must uncoat or remodel to allow passage of the preintegration complex through the nuclear pore. Under the conditions of our immunoblot assay, we observed a novel cleavage product that reacted with anti-CA antibodies and was approximately 17 kDa in mass (Fig. 3). The presence of this species correlated with the ability of mutants to produce cDNA, but it is also observed in an RT mutant that forms particles similar to those of the wt but does not produce cDNA (55; also data not shown). Thus, this CA species is not a byproduct of cDNA synthesis per se. In addition, this species was observed in the PR catalytic site mutant expressed for 24 h. Further analysis will be required to determine whether Ty3 PR can produce this product and whether this cleavage promotes cDNA synthesis or uncoating. Foamy virus- and Mason-Pfizer monkey virus-infected cells show evidence of cleavage in the respective CA proteins, which correlates with cDNA production (57, 78). In these cases, the cleavage is attributed to viral PR.

The striking phenotype of the K15A/E19A mutant indicated that the effects of loss of Ty3 CA function can persist after completion of cDNA synthesis. This mutant showed wt processing of Gag3, protection of mRNA and accumulation of wt amounts of cDNA but transposition barely above background. Possible post-reverse transcription defects include disruption of uncoating or nuclear targeting. The *Metaviridae* element Tf1 in *Schizosaccharomyces pombe* has a nuclear targeting signal in its major structural protein (25). Gag may also play a role in nuclear entry of retroviruses. Evidence is accumulating that CA uncoating may be the limiting step for preintegration complex entry into the nucleus (reviewed in reference 101). Mutations in HIV-1 CA that produce stable, reverse transcription-competent particles that are blocked for nuclear entry have been identified (27).

Summary. Analysis of the transposition intermediates of 26 CA domain mutants, together with previous work, allows us to propose the following more-detailed sequence of cytoplasmic events in Ty3 retrotransposition: (i) cytoplasmic expression; (ii) initiation of multimer formation independently of extensive P-body localization; (iii) association of Ty3 Gag3, Gag3-Pol3, and RNA with P-body components; (iv) protection of Ty3 RNA by assembly into VLPs; (v) proteolytic maturation by Ty3 PR; (vi) coalescence of small Ty3–P-body clusters into larger aggregates and cDNA synthesis; and (vii) remodeling of the VLP and nuclear entry.

Mutagenesis of the CA protein of the Ty3 retrotransposon showed that the NTD, including the MHR, is critical for particle formation and identified specific residues that influence P-body colocalization. In addition, in the case of two mutants that were affected in P-body localization, particle formation was reduced and defective. The availability of these and other Ty3 CA mutants provides valuable reagents for further elucidation of the VLP morphogenesis pathway. It has recently been reported that endogenous Jaagsiekte sheep retrovirus acts as a host restriction factor at least in part through relocalization of wt virus assembly (66). Improved understanding of intracellular retrovirus-like particle assembly may help provide insights into processes through which endogenous retroviruses can interfere with the assembly of their wt counterparts.

ACKNOWLEDGMENTS

This research was supported in part by funds from the National Institutes of Health (NIH), including Public Health Service grants GM33281 to S.S., GM68903 to G.W.H., and NSF EF-0330786, NIH CA112560, and NIH LM-07443-01 to P.B., and by the Institute for Genomics and Bioinformatics. The project was funded in part with funds to K.N. from the National Cancer Institute, NIH, under contract N01-CO-12400. N.B.-B. was supported by NIH grant T32 AI07319.

We thank M. Oakes for assistance with fluorescence microscopy. We thank Arlo Randall for helpful discussions. We thank Rhonda DaSilva, Image Analysis Laboratory, SAIC-Frederick, Inc., for assistance with EM.

REFERENCES

1. **Accola, M. A., B. Strack, and H. G. Gottlinger.** 2000. Efficient particle production by minimal Gag constructs which retain the carboxy-terminal domain of human immunodeficiency virus type 1 capsid-p2 and a late assembly domain. J. Virol. **74:**5395–5402.
2. **Adamczak, R., A. Porollo, and J. Meller.** 2005. Combining prediction of secondary structure and solvent accessibility in proteins. Proteins **59:**467–475.
3. **Adamson, C. S., and I. M. Jones.** 2004. The molecular basis of HIV capsid assembly—five years of progress. Ref. Med. Virol. **14:**107–121.
4. **Barklis, E., J. McDermott, S. Wilkens, S. Fuller, and D. Thompson.** 1998.

Organization of HIV-1 capsid proteins on a lipid monolayer. J. Biol. Chem. **273:**7177–7180.
5. **Barklis, E., J. McDermott, S. Wilkens, E. Schabtach, M. F. Schmid, S. Fuller, S. Karanjia, Z. Love, R. Jones, Y. J. Rui, X. M. Zhao, and D. Thompson.** 1997. Structural analysis of membrane-bound retrovirus capsid proteins. EMBO J. **16:**1199–1213.
6. **Beliakova-Bethell, N., C. Beckham, T. Giddings, Jr., M. Winey, R. Parker, and S. Sandmeyer.** 2006. Virus-like particles of the Ty3 retrotransposon assemble in association with P-body components. RNA **12:**94–101.
7. **Berman, H. M., J. Westbrook, Z. Feng, G. Gilliland, T. N. Bhat, H. Weissig, I. N. Shindyalov, and P. E. Bourne.** 2000. The Protein Data Bank. Nucleic Acids Res. **28:**235–242.
8. **Berthet-Colominas, C., S. Monaco, A. Novelli, G. Sibai, F. Mallet, and S. Cusack.** 1999. Head-to-tail dimers and interdomain flexibility revealed by the crystal structure of HIV-1 capsid protein (p24) complexed with a monoclonal antibody Fab. EMBO J. **18:**1124–1136.
9. **Bilanchone, V. W., J. A. Claypool, P. T. Kinsey, and S. B. Sandmeyer.** 1993. Positive and negative regulatory elements control expression of the yeast retrotransposon Ty3. Genetics **134:**685–700.
10. **Birkett, A. J., B. Yelamos, I. Rodriguez-Crespo, F. Gavilanes, and D. L. Peterson.** 1997. Cloning, expression, purification, and characterization of the major core protein (p26) from equine infectious anemia virus. Biochim. Biophys. Acta **1339:**62–72.
11. **Brengues, M., D. Teixeira, and R. Parker.** 2005. Movement of eukaryotic mRNAs between polysomes and cytoplasmic processing bodies. Science **310:**486–489.
12. **Briggs, J. A. G., M. N. Simon, I. Gross, H. G. Krausslich, S. D. Fuller, V. M. Vogt, and M. C. Johnson.** 2004. The stoichiometry of Gag protein in HIV-1. Nat. Struct. Mol. Biol. **11:**672–675.
13. **Bryson, K., L. J. McGuffin, R. L. Marsden, J. J. Ward, J. S. Sodhi, and D. T. Jones.** 2005. Protein structure prediction servers at University College London. Nucleic Acids Res. **33:**W36–W38.
14. **Burstein, H., D. Bizub, and A. M. Skalka.** 1991. Assembly and processing of avian retroviral *gag* polyproteins containing linked protease dimers. J. Virol. **65:**6165–6172.
15. **Butterfield-Gerson, K. L., L. Z. Scheifele, E. P. Ryan, A. K. Hopper, and L. J. Parent.** 2006. Importin-β family members mediate alpharetrovirus Gag nuclear entry via interactions with matrix and nucleocapsid. J. Virol. **80:**1798–1806.
16. **Cairns, T. M., and R. C. Craven.** 2001. Viral DNA synthesis defects in assembly competent Rous sarcoma virus CA mutants. J. Virol. **75:**242–250.
17. **Campos-Olivas, R., J. L. Newman, and M. F. Summers.** 2000. Solution structure and dynamics of the Rous sarcoma virus capsid protein and comparison with capsid proteins of other retroviruses. J. Mol. Biol. **296:**633–649.
18. **Cheng, J., and P. Baldi.** 2006. A machine learning information retrieval approach to protein fold recognition. Bioinformatics **22:**1456–1463.
19. **Cheng, J., A. Z. Randall, M. J. Sweredoski, and P. Baldi.** 2005. SCRATCH: a protein structure and structural feature prediction server. Nucleic Acids Res. **33:**W72–W76.
20. **Cheynet, V., B. Verrier, and F. Mallet.** 1993. Overexpression of HIV-1 proteins in *Escherichia coli* by a modified expression vector and their one-step purification. Protein Expr. Purif. **4:**367–372.
21. **Coffin, J. M., S. H. Hughes, and H. E. Varmus (ed.).** 1997. Retroviruses. Cold Spring Harbor Laboratory Press, Plainview, NY.
22. **Coller, J. M., M. Tucker, U. Sheth, M. A. Valencia-Sanchez, and R. Parker.** 2001. The DEAD box helicase, Dhh1p, functions in mRNA decapping and interacts with both the decapping and deadenylase complexes. RNA **7:**1717–1727.
23. **Craven, R. C., A. E. Leure-DuPree, C. R. Erdie, C. B. Wilson, and J. W. Wills.** 1993. Necessity of the spacer peptide between CA and NC in the Rous sarcoma virus Gag protein. J. Virol. **67:**6246–6252.
24. **Curcio, M. J., and D. J. Garfinkel.** 1991. Regulation of retrotransposition in *Saccharomyces cerevisiae*. Mol. Microbiol. **5:**1823–1829.
25. **Dang, V. D., and H. L. Levin.** 2000. Nuclear import of the retrotransposon Tf1 is governed by a nuclear localization signal that possesses a unique requirement for the FXFG nuclear pore factor Nup124p. Mol. Cell. Biol. **20:**7798–7812.
26. **Demirov, D. G., and E. O. Freed.** 2004. Retrovirus budding. Virus Res. **106:**87–102.
27. **Dismuke, D. J., and C. Aiken.** 2006. Evidence for a functional link between uncoating of the human immunodeficiency virus type 1 core and nuclear import of the viral preintegration complex. J. Virol. **80:**3712–3720.
28. **Dorfman, T., A. Bukovsky, A. Ohagen, S. Hoglund, and H. G. Gottlinger.** 1994. Functional domains of the capsid protein of human immunodeficiency virus type 1. J. Virol. **68:**8180–8187.
29. **Ebbets-Reed, D., S. Scarlata, and C. A. Carter.** 1996. The major homology region of the HIV-1 gag precursor influences membrane affinity. Biochemistry **35:**14268–14275.
30. **Eickbush, T., and H. Malik.** 2002. Origins and evolution of retrotransposons, p. 1111–1144. *In* N. Craig, R. Craigie, M. Gellert, and A. Lambowitz (ed.), Mobile DNA II. ASM Press, Washington, DC.
31. **Forshey, B. M., U. von Schwedler, W. I. Sundquist, and C. Aiken.** 2002. Formation of a human immunodeficiency virus type 1 core of optimal stability is crucial for viral replication. J. Virol. **76:**5667–5677.
32. **Franke, E. K., H. E. H. Yuan, K. L. Bossolt, S. P. Goff, and J. Luban.** 1994. Specificity and sequence requirements for interactions between various retroviral Gag proteins. J. Virol. **68:**5300–5305.
33. **Fuller, S. D., T. Wilk, B. E. Gowen, H. G. Krausslich, and V. M. Vogt.** 1997. Cryo-electron microscopy reveals ordered domains in the immature HIV-1 particle. Curr. Biol. **7:**729–738.
34. **Gamble, T. R., F. F. Vajdos, S. H. Yoo, D. K. Worthylake, M. Houseweart, W. I. Sundquist, and C. P. Hill.** 1996. Crystal structure of human cyclophilin A bound to the amino-terminal domain of HIV-1 capsid. Cell **87:**1285–1294.
35. **Gamble, T. R., S. H. Yoo, F. F. Vajdos, U. K. vonSchwedler, D. K. Worthylake, H. Wang, J. P. McCutcheon, W. I. Sundquist, and C. P. Hill.** 1997. Structure of the carboxyl-terminal dimerization domain of the HIV-1 capsid protein. Science **278:**849–853.
36. **Ganser, B. K., A. C. Cheng, W. I. Sundquist, and M. Yeager.** 2003. Three-dimensional structure of the M-MuLV CA protein on a lipid monolayer: a general model for retroviral capsid assembly. EMBO J. **22:**2886–2892.
37. **Ganser-Pornillos, B. K., U. K. von Schwedler, K. M. Stray, C. Aiken, and W. I. Sundquist.** 2004. Assembly properties of the human immunodeficiency virus type 1 CA protein. J. Virol. **78:**2545–2552.
38. **Ginalski, K., M. von Grotthuss, N. V. Grishin, and L. Rychlewski.** 2004. Detecting distant homology with Meta-BASIC. Nucleic Acids Res. **32:**W576–W581.
39. **Gitti, R. K., B. M. Lee, J. Walker, M. F. Summers, S. Yoo, and W. I. Sundquist.** 1996. Structure of the amino-terminal core domain of the HIV-1 capsid protein. Science **273:**231–235.
40. Reference deleted.
41. **Hansen, L. J., D. L. Chalker, K. J. Orlinsky, and S. B. Sandmeyer.** 1992. Ty3 *GAG3* and *POL3* genes encode the components of intracellular particles. J. Virol. **66:**1414–1424.
42. **Hansen, L. J., D. L. Chalker, and S. B. Sandmeyer.** 1988. Ty3, a yeast retrotransposon associated with tRNA genes, has homology to animal retroviruses. Mol. Cell. Biol. **8:**5245–5256.
43. **Hoffman, C. S., and F. Winston.** 1987. A ten-minute DNA preparation from yeast efficiently releases autonomous plasmids for transformation of *Escherichia coli*. Gene **57:**267–272.
44. **Huang, M. J., and M. A. Martin.** 1997. Incorporation of $Pr160^{gag\text{-}pol}$ into virus particles requires the presence of both the major homology region and adjacent C-terminal capsid sequences within the Gag-Pol polyprotein. J. Virol. **71:**4472–4478.
45. **Irwin, B., M. S. Aye, P. Baldi, N. Beliakova-Bethell, H. Cheng, Y. Dou, W. Liou, and S. Sandmeyer.** 2005. Retroviruses and yeast retrotransposons use overlapping sets of host genes. Genome Res. **15:**641–654.
46. **Ivanov, D., J. R. Stone, J. L. Maki, T. Collins, and G. Wagner.** 2005. Mammalian SCAN domain dimer is a domain-swapped homolog of the HIV capsid C-terminal domain. Mol. Cell **17:**137–143.
47. **Jaroszewski, L., L. Rychlewski, Z. Li, W. Li, and A. Godzik.** 2005. FFAS03: a server for profile-profile sequence alignments. Nucleic Acids Res. **33:**W284–W288.
48. **Jin, Z. M., L. Jin, D. L. Peterson, and C. L. Lawson.** 1999. Model for lentivirus capsid core assembly based on crystal dimers of EIAV p26. J. Mol. Biol. **286:**83–93.
49. **Karplus, K., K. Sjolander, C. Barrett, M. Cline, D. Haussler, R. Hughey, L. Holm, and C. Sander.** 1997. Predicting protein structure using hidden Markov models. Proteins **1**(Suppl.)**:**134–139.
50. **Khorasanizadeh, S., R. Campos-Olivas, and M. F. Summers.** 1999. Solution structure of the capsid protein from the human T-cell leukemia virus type-I. J. Mol. Biol. **291:**491–505.
51. **Kingston, R. L., T. Fitzon-Ostendorp, E. Z. Eisenmesser, G. W. Schatz, V. M. Vogt, C. B. Post, and M. G. Rossmann.** 2000. Structure and self-association of the Rous sarcoma virus capsid protein. Structure **8:**617–628.
52. **Kinsey, P., and S. Sandmeyer.** 1995. Ty3 transposes in mating populations of yeast: a novel transposition assay for Ty3. Genetics **139:**81–94.
53. **Kirchner, J., and S. B. Sandmeyer.** 1993. Proteolytic processing of Ty3 proteins is required for transposition. J. Virol. **67:**19–28.
54. **Kirchner, J., S. B. Sandmeyer, and D. B. Forrest.** 1992. Transposition of a Ty3 *GAG3-POL3* fusion mutant is limited by availability of capsid protein. J. Virol. **66:**6081–6092.
55. **Kuznetsov, Y. G., M. Zhang, T. M. Menees, A. McPherson, and S. Sandmeyer.** 2005. Investigation by atomic force microscopy of the structure of Ty3 retrotransposon particles. J. Virol. **79:**8032–8045.
56. **Larson, D. R., Y. M. Ma, V. M. Vogt, and W. W. Webb.** 2003. Direct measurement of Gag-Gag interaction during retrovirus assembly with FRET and fluorescence correlation spectroscopy. J. Cell Biol. **162:**1233–1244.
57. **Lehmann-Che, J., M. L. Giron, O. Delelis, M. Lochelt, P. Bittoun, J. Tobaly-Tapiero, H. de The, and A. Saib.** 2005. Protease-dependent uncoating of a complex retrovirus. J. Virol. **79:**9244–9253.

58. **Li, S., C. P. Hill, W. I. Sundquist, and J. T. Finch.** 2000. Image reconstructions of helical assemblies of the HIV-1CA protein. Nature **407:**409–413.
59. **Lin, J. H., and H. L. Levin.** 1998. Reverse transcription of a self-primed retrotransposon requires an RNA structure similar to the U5-IR stem-loop of retroviruses. Mol. Cell. Biol. **18:**6859–6869.
60. **Mammano, F., A. Ohagen, S. Hoglund, and H. G. Gottlinger.** 1994. Role of the major homology region of human immunodeficiency virus type 1 in virion morphogenesis. J. Virol. **68:**4927–4936.
61. **Menees, T. M., and S. B. Sandmeyer.** 1994. Transposition of the yeast retrovirus-like element Ty3 is dependent on the cell cycle. Mol. Cell. Biol. **14:**8229–8240.
62. **Momany, G., L. C. Kovari, A. J. Prongay, W. Keller, R. K. Gitti, B. M. Lee, A. E. Gorbalenya, L. Tong, J. McClure, L. S. Ehrlich, M. F. Summers, C. Carter, and M. G. Rossmann.** 1996. Crystal structure of dimeric HIV-1 capsid protein. Nat. Struct. Biol. **3:**763–770.
63. **Monaco-Malbet, S., C. Berthet-Colominas, A. Novelli, N. Battai, N. Piga, V. Cheynet, F. Mallet, and S. Cusack.** 2000. Mutual conformational adaptations in antigen and antibody upon complex formation between an Fab and HIV-1 capsid protein p24. Structure **8:**1069–1077.
64. **Morita, E., and W. I. Sundquist.** 2004. Retrovirus budding. Annu. Rev. Cell Dev. Biol. **20:**395–425.
65. **Mortuza, G. B., L. F. Haire, A. Stevens, S. J. Smerdon, J. P. Stoye, and I. A. Taylor.** 2004. High-resolution structure of a retroviral capsid hexameric amino-terminal domain. Nature **431:**481–485.
66. **Murcia, P. R., F. Arnaud, and M. Palmarini.** 2007. The transdominant endogenous retrovirus enJS56A1 associates with and blocks intracellular trafficking of Jaagsiekte sheep retrovirus Gag. J. Virol. **81:**1762–1772.
67. **Nermut, M. V., D. J. Hockley, P. Bron, D. Thomas, W. H. Zhang, and I. M. Jones.** 1998. Further evidence for hexagonal organization of HIV gag protein in prebudding assemblies and immature virus-like particles. J. Struct. Biol. **123:**143–149.
68. **Ohlson, T., B. Wallner, and A. Elofsson.** 2004. Profile-profile methods provide improved fold-recognition: a study of different profile-profile alignment methods. Proteins **57:**188–197.
69. **Orlinsky, K., J. Gu, M. Hoyt, S. Sandmeyer, and T. Menees.** 1996. Mutations in the Ty3 major homology region affect viruslike particle morphogenesis. J. Virol. **70:**3440–3448.
70. **Orlinsky, K. J., and S. B. Sandmeyer.** 1994. The Cys-His motif of Ty3 NC can be contributed by Gag3 or Gag3-Pol3 polyproteins. J. Virol. **68:**4152–4166.
71. **Perlman, M., and M. D. Resh.** 2006. Identification of an intracellular trafficking and assembly pathway for HIV-1 gag. Traffic **7:**731–745.
72. **Provitera, P., A. Goff, A. Harenberg, F. Bouamr, C. Carter, and S. Scarlata.** 2001. Role of the major homology region in assembly of HIV-1 Gag. Biochemistry **40:**5565–5572.
73. **Reicin, A. S., S. Paik, R. D. Berkowitz, J. Luban, I. Lowy, and S. Goff.** 1995. Linker insertion mutations in the human immunodeficiency virus type 1 *gag* gene: effects on virion particle assembly, release, and infectivity. J. Virol. **69:**642–650.
74. **Resh, M. D.** 2005. Intracellular trafficking of HIV-1 Gag: how Gag interacts with cell membranes and makes viral particles. AIDS Rev. **7:**84–91.
75. **Ribet, D., F. Harper, M. Dewannieux, G. Pierron, and T. Heidmann.** 2007. Murine MusD retrotransposon: structure and molecular evolution of an "intracellularized" retrovirus. J. Virol. **81:**1888–1898.
76. **Rost, B., G. Yachdav, and J. F. Liu.** 2004. The PredictProtein server. Nucleic Acids Res. **32:**W321–W326.
77. **Roth, J. F.** 2000. The yeast Ty virus-like particles. Yeast **16:**785–795.
78. **Rumlova, M., T. Ruml, J. Pohl, and I. Pichova.** 2003. Specific in vitro cleavage of Mason-Pfizer monkey virus capsid protein: evidence for a potential role of retroviral protease in early stages of infection. Virology **310:**310–318.
79. **Sali, A., and T. L. Blundell.** 1993. Comparative protein modelling by satisfaction of spatial restraints. J. Mol. Biol. **234:**779–815.
80. **Sambrook, J., and D. Russell.** 2001. Molecular cloning: a laboratory manual. Cold Spring Harbor Laboratory Press, Cold Spring Harbor, NY.
81. **Sandmeyer, S. B., M. Aye, and T. M. Menees.** 2002. Ty3: a position-specific, gypsylike element in *Saccharomyces cerevisiae*, p. 663–682. *In* N. L. Craig, R. Craigie, M. Gellert, and A. M. Lambowitz (ed.), Mobile DNA II. ASM Press, Washington, DC.
82. **Scarlata, S., and C. Carter.** 2003. Role of HIV-1 Gag domains in viral assembly. Biochim. Biophys. Acta **1614:**62–72.
83. **Scheifele, L. Z., R. A. Garbitt, J. D. Rhoads, and L. J. Parent.** 2002. Nuclear entry and CRM1-dependent nuclear export of the Rous sarcoma virus Gag polyprotein. Proc. Natl. Acad. Sci. USA **99:**3944–3949.
84. **Schiestl, R. H., and D. R. Gietz.** 1989. High efficiency transformation of intact yeast cells using single stranded nucleic acids as a carrier. Curr. Genet. **16:**339–346.
85. **Sfakianos, J. N., R. A. LaCasse, and E. Hunter.** 2003. The M-PMV cytoplasmic targeting-retention signal directs nascent Gag polypeptides to a pericentriolar region of the cell. Traffic **4:**660–670.

85a. **Sherman, F.** 2002. Getting started with yeast. Methods Enzymol. **350B:**3–41.

86. **Sheth, U., and R. Parker.** 2003. Decapping and decay of messenger RNA occur in cytoplasmic processing bodies. Science **300:**805–808.
87. **Srinivasakumar, N., M.-L. Hammarskjold, and D. Rekosh.** 1995. Characterization of deletion mutations in the capsid region of human immunodeficiency virus type 1 that affect particle formation and Gag-Pol precursor incorporation. J. Virol. **69:**6106–6114.
88. **Strambio-de-Castillia, C., and E. Hunter.** 1992. Mutational analysis of the major homology region of Mason-Pfizer monkey virus by use of saturation mutagenesis. J. Virol. **66:**7021–7032.
89. **Teysset, L., V. D. Dang, M. K. Kim, and H. L. Levin.** 2003. A long terminal repeat-containing retrotransposon of *Schizosaccharomyces pombe* expresses a Gag-like protein that assembles into virus-like particles which mediate reverse transcription. J. Virol. **77:**5451–5463.
90. **Thompson, J. D., D. G. Higgins, and T. J. Gibson.** 1994. CLUSTAL W: improving the sensitivity of progressive multiple sequence alignment through sequence weighting, position-specific gap penalties and weight matrix choice. Nucleic Acids Res. **22:**4673–4680.
91. **Tritel, M., and M. D. Resh.** 2000. Kinetic analysis of human immunodeficiency virus type 1 assembly reveals the presence of sequential intermediates. J. Virol. **74:**5845–5855.
92. **Vida, T. A., and S. D. Emr.** 1995. A new vital stain for visualizing vacuolar membrane dynamics and endocytosis in yeast. J. Cell Biol. **128:**779–792.
93. **von Schwedler, U. K., T. L. Stemmler, V. Y. Klishko, S. Li, K. H. Albertine, D. R. Davis, and W. I. Sundquist.** 1998. Proteolytic refolding of the HIV-1 capsid protein amino-terminus facilitates viral core assembly. EMBO J. **19:**2391.
94. **von Schwedler, U. K., K. M. Stray, J. E. Garrus, and W. I. Sundquist.** 2003. Functional surfaces of the human immunodeficiency virus type 1 capsid protein. J. Virol. **77:**5439–5450.
95. **Wang, C.-T., and E. Barklis.** 1993. Assembly, processing, and infectivity of human immunodeficiency virus type 1 Gag mutants. J. Virol. **67:**4264–4273.
96. **Weldon, R. A., Jr., and J. W. Wills.** 1993. Characterization of a small (25-kilodalton) derivative of the Rous sarcoma virus Gag protein competent for particle release. J. Virol. **67:**5550–5561.
97. **Wichroski, M. J., G. B. Robb, and T. M. Rana.** 2006. Human retroviral host restriction factors APOBEC3G and APOBEC3F localize to mRNA processing bodies. PLoS Pathog. **2:**e41.
98. **Wilk, T., and S. D. Fuller.** 1999. Towards the structure of the human immunodeficiency virus: divide and conquer? Curr. Opin. Cell Biol. **9:**231–243.
99. **Wills, J. W., C. E. Cameron, C. B. Wilson, Y. Xiang, R. P. Bennett, and J. Leis.** 1994. An assembly domain of the Rous sarcoma virus Gag protein required late in budding. J. Virol. **68:**6605–6618.
100. **Wills, J. W., and R. C. Craven.** 1991. Form, function, and use of retroviral Gag proteins. AIDS **5:**639–654.
101. **Yamashita, M., and M. Emerman.** 2006. Retroviral infection of non-dividing cells: old and new perspectives. Virology **344:**88–93.
102. **Yeager, M., E. M. Wilson-Kubalek, S. G. Weiner, P. O. Brown, and A. Rein.** 1998. Supramolecular organization of immature and mature murine leukemia virus revealed by electron cryo-microscopy: implications for retroviral assembly mechanisms. Proc. Natl. Acad. Sci. USA **95:**7299–7304.
103. **Yu, S. F., S. W. Eastman, and M. L. Linial.** 2006. Foamy virus capsid assembly occurs at a pericentriolar region through a cytoplasmic targeting/retention signal in gag. Traffic **7:**966–977.